Master in Chemical Engineering

Steam Methane Reforming: Process Intensification through NETmix® Technology

A Master's dissertation

of

Lígia Beatriz Sá Azevedo Dias

Developed within the course of dissertation

held in

Associate Laboratory LSRE-LCM

Supervisor at FEUP: **Prof. José Carlos Lopes**

Departamento de Engenharia Química

July 2018

Agradecimentos

Gostaria de começar por agradecer a todas as pessoas que me acompanharam no meu percurso, tanto académico como pessoal, e que me apoiaram sempre que precisei.

Quero agradecer, especialmente, ao meu orientador, Professor José Carlos Lopes, e à Professora Madalena Dias pela oportunidade de integrar o grupo de investigação e pelas condições que proporcionaram para desenvolver a tese sobre um tema tão cativante. O seu apoio e disponibilidade foram imprescindíveis neste período de crescimento académico.

Gostaria também de agradecer ao Doutor Marcelo Costa e à Doutora Mariana Domingos pelo pronto esclarecimento das dúvidas que foram surgindo e pelas sugestões que valorizaram o meu trabalho e me permitiram evoluir. Trabalhar com investigadores experientes foi muito gratificante.

Gostaria de agradecer à Fundação para a Ciência e a Tecnologia pela concessão da bolsa de iniciação científica usufruída durante o período da dissertação, celebrada no âmbito do projeto LSRE-LCM-UID/EQU/50020 - POCI-01-0145-FEDER-006984.

Gostaria de agradecer aos meus colegas e amigos, especialmente ao Frederico e à Catarina, que me acompanharam nestes anos académicos e que tornaram este percurso mais divertido.

Gostaria de agradecer ainda à minha família, especialmente aos meus pais, por todo o apoio e por estarem sempre ao meu lado quando mais preciso. Obrigada por me ensinarem a dar sempre o meu melhor, tudo o que sou hoje devo-o a vocês.

Este trabalho foi financiado por: Projeto POCI-01-0145-FEDER-006984 - Laboratório Associado LSRE-LCM - financiado pelo Fundo Europeu de Desenvolvimento Regional (FEDER), através do COMPETE2020 – Programa Operacional Competitividade e Internacionalização (POCI) e por fundos nacionais através da Fundação para a Ciência e a Tecnologia I.P.

Abstract

This dissertation aims to simulate an industrial Steam Methane Reforming (SMR) process using a NETmix® device as the core unit of the process, the reforming reactor, instead of a typical fired steam reformer and shift reactor. The simulation software chosen was Aspen Plus®, which was also used to simulate the performance of a rhodium catalyst for the reactor configuration in question.

This work presents, in sequential order, the steps taken to define the process flowsheet of an industrial SMR process with the NETmix® technology. First, the available kinetic expressions for a rhodium supported catalyst are introduced in the simulation software and the simulated results validated against previously published experimental data. Then, the catalyst composition is adapted by removing its support to resemble the case where a catalyst is applied using the sputtering technique. Reaction rate equations are modified in accordance with the catalyst adaptations and the absence of mass diffusion limitations is confirmed to assess the applicability of this technique in a LabNETmix reactor. Finally, the global flowsheet for a SMR process is built, based on a reference hydrogen plant from SIAD S.p.A. and with a scaled-up LabNETmix reactor. An energy integration network is included in the process flowsheet and operational and capital expenditures estimated through an OPEX and CAPEX analysis.

The simulated industrial SMR plant with a 22.0 m^3 LabNETmix is capable of an hourly syngas production of 5.57 tonnes, with a methane conversion of 78 % and a reactor heat duty of 15.3 MW, to feed a Fischer-Tropsch plant producing 250 barrels per day of synthetic fuel. The adapted catalyst consists of a thin layer of rhodium with 200 nm thickness in each of the heat transfer walls of the LabNETmix network and has fewer mass diffusivity limitations when compared to the catalyst retrieved from literature that served as a base case. The syngas produced presents a H_2/CO ratio of 2, which is the ideal value for a cobalt-based Fischer-Tropsch process for production of synthetic fuels. The foreseen costs for the simulated SMR plant are US$ 156 per tonne of syngas of capital expenditure (CAPEX) and US$ 82 per tonne of syngas of operating costs (OPEX), totalizing US$ 238 for each tonne of hydrogen and carbon monoxide produced over the 30 years of economical lifespan of the SMR industrial plant.

Keywords: reforming, syngas, kinetics, NETmix, simulation.

Resumo

Esta dissertação tem como objetivo a simulação de um processo industrial de *reforming* de metano com vapor (*Steam Methane Reforming*) usando um dispositivo NETmix® como núcleo do processo, o reator de *reforming*, em vez de um *reformer* a vapor típico e de um reator de *shift*. O *software* de simulação escolhido foi o programa Aspen Plus®, que também foi usado para simular o desempenho de um catalisador de ródio para o reator em questão.

Ao longo deste trabalho, e de forma sequencial, são descritas as diversas tarefas que foram realizadas para obter o *flowsheet* final de uma planta industrial de SMR. Em primeiro lugar, as expressões cinéticas para um catalisador de ródio suportado são introduzidas no *software* de simulação e os resultados simulados validados por comparação com dados experimentais disponíveis na literatura. Em seguida, a composição do catalisador é adaptada através da remoção do suporte de forma a se assemelhar a um catalisador aplicado usando a técnica de *sputtering*. As equações cinéticas são adaptadas de acordo com as alterações ao catalisador e a ausência de limitações difusionais é confirmada para testar sua aplicabilidade a um reator LabNETmix. Finalmente, um *flowsheet* global para um processo SMR é criado, baseado numa planta industrial de hidrogénio da SIAD S.p.A. como referência e a operar com um reator LabNETmix de grande escala. Uma rede de integração energética é incluída no *flowsheet* do processo e são feitas estimativas de custos operacionais e de capital através de uma análise de OPEX e CAPEX.

A planta SMR industrial simulada opera com um LabNETmix de 22.0 m^3 capaz de uma produção horária de gás de síntese de 5.57 toneladas com uma conversão de metano de 78 % e uma exigência térmica de 15.3 MW. O catalisador adaptado consiste numa fina camada de ródio com 200 nm de espessura colocada em cada uma das paredes de transferência de calor da rede LabNETmix e possui menos limitações difusionais quando comparado com o catalisador-base referido na literatura. O gás de síntese produzido apresenta uma razão H_2/CO de 2, que é o valor ideal para um processo Fischer-Tropsch com catalisador de cobalto para a produção de combustíveis sintéticos. Os custos previstos para a planta SMR simulada são de US$ 156 por tonelada de gás de síntese em custos de capital (CAPEX) e US$ 82 por tonelada de gás de síntese em custos operacionais (OPEX), totalizando US$ 238 por cada tonelada de hidrogénio e monóxido de carbono produzida durante os 30 anos de vida útil da planta industrial SMR.

Declaration

I hereby declare, on my word of honour, that this work is original and that all non-original contributions were properly referenced with source identification.

Lígia Beatriz Sá Azevedo Dias

Julho 2018

Index

List of Figures

List of Tables

Notation and Glossary

A	Pre-exponential factor for direct reaction	$kmol \cdot m_{cat}^{-3} \cdot s^{-1} \cdot bar^{-2}$
A'	Pre-exponential factor for inverse reaction	$kmol \cdot m_{cat}^{-3} \cdot s^{-1} \cdot bar^{-2}$
$Area$	Cross section area of the catalyst layer	cm^2
C_{equip}	Equipment total direct cost	US$
C^s	Concentration at surface	$mol \cdot cm^{-3}$
D	LabNETmix chamber's diameter	mm
$\mathcal{D}$	Molecular diffusion coefficient	$cm^2 \cdot s^{-1}$
d	LabNETmix chamber's diameter/depth	mm
$\mathcal{D}_{eff}$	Effective diffusivity	$cm^2 \cdot s^{-1}$
$\mathcal{D}_k$	Knudsen diffusion	$m^2 \cdot s^{-1}$
E	Activation energy for direct reaction	$J \cdot kmol^{-1}$
E'	Activation energy for inverse reaction	$J \cdot kmol^{-1}$
f	Normalized concentration	
H	Enthalpy	$kJ \cdot mol^{-1}$
$\hat{h}$	Specific heat transfer capacity	$W \cdot m^{-3} \cdot K^{-1}$
k	Rate constant	$kmol \cdot m_{cat}^{-3} \cdot s^{-1} \cdot bar^{-2}$
k_B	Boltzmann constant	$J \cdot K^{-1}$
K_1	Equilibrium constant for SMR reaction	bar^2
K_2	Equilibrium constant for WGS reaction	
L	Distance from centres of two adjacent LabNETmix chambers	mm
l	Layer thickness	m
$\widetilde{M}$	Molecular weight	$kg \cdot mol^{-1}$
m	Mean free path	m
$N_{hours/year}$	Annual operating hours	
N_{years}	Economical lifespan	
n_x	Number of rows of the LabNETmix	
n_y	Number of inlets and outlets of the LabNETmix	
P	Absolute pressure	bar
p	Partial pressure	bar
$\dot{P}$	Productivity	$tonne \cdot h^{-1}$
Q_C	Cold utility requirement	MW
Q_H	Hot utility requirement	MW
R	Universal gas constant	$J \cdot mol^{-1}\ K^{-1}$
r	Reaction rate	$kmol \cdot m_{cat}^{-3} \cdot s^{-1}$
r'	Pore radius	m
S	Selectivity	
T	Temperature	Kelvin
V	Volume	cm^3
W	Mass flow	$kg \cdot h^{-1}$
X	Molar conversion	
x	Normalized position in the catalyst layer	
y	Molar fraction	
z	Position within the catalyst layer	cm

Greek Letters

Δ	Change/Difference	
δ	Diameter of the sphere	m
ε	Porosity	
η	Effectiveness factor	

ρ	Density	$g \cdot cm^{-3}$
σ	Collision diameter	Å
Φ	Thiele modulus	
φ	Flux of methane	$mol \cdot s^{-1} \cdot cm^{-2}$
Ω	Collision integral	
ω	LabNETmix channel's height	mm

Indexes

cat	Catalyst
CH_4	Methane
CO	Carbon Monoxide
CO_2	Carbon Dioxide
f	Felt
H_2O	Water
i	Reaction number (i = 1, 2)
in reactor	Reactor inlet
j	Reaction component (j = 1, 2)
k	Equipment number (k = 1 to 23)
layer	Layer
max	Maximum
min	Minimum
N	Normal
obs	Observed
out reactor	Reactor outlet
p	Particle
s	Solid
syngas	Syngas (H_2+CO)
t,s	True, at surface conditions
z	Zeolite

List of Acronyms

ASME	American Society of Mechanical Engineers
CAPEX	Capital Expenditure
COP	Coefficient of Performance
GTL	Gas-to-Liquids
HTS	High Temperature Shift
IUPAC	International Union of Pure and Applied Chemistry
LSRE	Laboratory of Separation and Reaction Engineering
LTS	Low Temperature Shift
OPEX	Operating Expenditure
PSA	Pressure Swing Adsorption
RK23	$2^{nd}/3^{rd}$ order Runge-Kutta Method
SIAD	Società Italiana Acetilene e Derivati
SLPM	Standard Litres per Minute
SMR	Steam Methane Reforming
STP	Standard Temperature and Pressure Conditions
TEMA	Tubular Exchanger Manufacturers Association
WGS	Water-Gas Shift

1 Introduction

1.1 Framing and presentation of the work

Nowadays, the concern with air pollution and climate change due to fossil fuel dependence is on the rise. Traditional fuels, such as diesel or coal, have been used throughout the years as energy providers, mainly through combustion, having a significant impact on climate change. An alternative for the traditional fuels is the use of synthetic hydrocarbon-based fuels, which burn "cleaner", i.e., produce less carbon dioxide and SO_x compounds than conventional fuels. Steam Methane Reforming (SMR) is the first step to produce these synthetic fuels, by converting methane into carbon monoxide and hydrogen (syngas), which can be fed to a Fischer-Tropsch process, responsible for generating heavier chains of hydrocarbons from this two light compounds.

The main goal of this work is to assess the possibility of operating a Steam Methane Reforming process, using the NETmix® technology as a substitute for the typical large fired reformers and shift reactors, including the simulation of a working SMR industrial plant with this new technology incorporated. The NETmix® technology consists on a network of mixing chambers interconnected by transport channels that allow mixing fluids in a controlled way without using any external mechanical mixing equipment. It is believed that NETmix® may be a solution for downsizing reforming equipment while addressing the existing heat and mass transfer problems in the typical reforming process related to the catalyst and the large reactor dimensions. The downsizing of reformers is of high interest since it enables the offshore exploration of stranded and remote natural gas reserves, avoiding the construction of long and expensive pipelines.

For this simulation-based dissertation, three software programs from AspenTech® were used, namely Aspen Plus® V9, Aspen Energy Analyzer® V9 and Aspen Process Economic Analyzer V9. The first goal is to introduce available kinetic expressions into the simulation software and validate the resulting simulated results against experimental data previously published. Next, the catalyst and the kinetic expressions were adapted to simulate the performance of a rhodium catalyst applied onto a LabNETmix reactor by sputtering technique and the presence of mass diffusivity limitation on the new catalyst is investigated. The final goal is to create a flowsheet of an industrial SMR plant operating with a LabNETmix reactor, with the purpose of producing enough syngas to feed a Fischer-Tropsch industrial plant with a 250 barrels per day capacity, and assess its CAPEX (capital expenditure) and OPEX (operating expenditure) values.

1.2 Contributions of the Work

This work represents the first approach to the use of a NETmix® reactor for Steam Methane Reforming. All the calculations and simulations were done by me, except the RK23 algorithm used to draw the methane concentration profile inside the catalyst, which was developed by Prof. M.R.N. Costa and Prof. Madalena Dias.

1.3 Organization of the thesis

This dissertation begins with the presentation of the Steam Methane Reforming process in Chapter 2. In this section, a global overview of the process, thermodynamics involved and catalysts used is given to introduce the reader to the theme.

In Chapter 3, kinetics for a rhodium-based catalyst are reproduced and validated using Aspen Plus®. Also, the catalyst composition is modified to enable its application through sputtering. Additionally, the potential presence of internal mass transfer/diffusion limitations is evaluated.

In Chapter 4, the process flowsheet of a SMR industrial plant with a LabNETmix reactor is described in detail. The simulated process plant is subdivided in five different subsections: natural gas pre-treatment; steam generation; reforming; separation and purification; and energy integration network. The final section of this chapter ends with CAPEX and OPEX estimations based on the flowsheet created.

This document also includes six appendixes where additional information regarding Water-Gas-Shift reaction and the rhodium supported catalyst can be found. Further auxiliary calculations, a VBA code transcription, process energy integration network and detailed equipment costs are also presented in these final pages.

2 Context and State of the art

The present work aims to evaluate the applicability of the NETmix® technology for the production of synthesis gas (or syngas), by simulating a Steam Methane Reforming (SMR) process.

2.1 Steam Methane Reforming

Steam reforming of hydrocarbons is the dominating process for the production of hydrogen, especially for refineries (Aasberg-Petersen et al., 2004). In recent years, steam reforming is being studied as a way of converting the primary feed into a gas suitable for synthetic fuels production and for fuel cells (Aasberg-Petersen et al., 2004).

2.1.1 Thermodynamics and Chemistry

Steam methane reforming of natural gas is the main commercial process for synthesis gas production. In this process, methane reacts with steam to produce a mixture of hydrogen, carbon dioxide and carbon monoxide. This gas phase reaction is highly endothermic and is performed in large fired reformers at high temperatures (800-1000 °C), high pressures (around 20-40 bar, which do not favour the reaction but are imposed by the process demands of the step which typically follows SMR, like Fischer-Tropsch) and with H_2O/CH_4 in the range of 1.8 to 4. The SMR is a well-known and controlled process but its overall efficiency is limited by heat losses (Mbodji et al., 2012).

Table 2-1 presents the chemical reactions expected to occur when performing steam methane reforming.

Table 2-1. Gas phase reactions in steam reforming of methane and reactions leading to carbon formation (Aasberg-Petersen et al., 2004, Nikoo and Amin, 2011).

		Reaction	ΔH_{298}(kJ·mol^{-1})
(2.1)	SMR	$CH_4 + H_2O \rightleftharpoons CO + 3H_2$	+206
(2.2)	Water-gas shift	$CO + H_2O \rightleftharpoons CO_2 + H_2$	-41.0
(2.3)	Methane cracking	$CH_4 \rightleftharpoons C + 2H_2$	+74.9
(2.4)	Boudouard reaction	$2CO \rightleftharpoons C + CO_2$	-172.4
(2.5)	CO reduction	$H_2 + CO \rightleftharpoons C + H_2O$	-131.3
(2.6)	Steam reforming (for n>1)	$C_nH_m + n\,H_2O \rightarrow (n + m/2)\,H_2 + n\,CO$	-

Usually, the steam methane reforming is operated far from equilibrium and the water-gas shift reaction is considered at equilibrium at high temperature and pressure conditions. The process usually occurs at the gas supply pressure, greater than atmospheric, to save energy for compression of the resulting gaseous mixture of larger volume (syngas used for Fischer-Tropsch, typically operated at 30 bar) and also because a lower volumetric flow requires smaller equipment. To compensate the high pressure, the temperature or the steam/carbon ratio (typically 3) are increased to improve methane conversion and carbon removal (Rostrup-Nielsen, 2008, Baltrusaitis and Luyben, 2015).

The main problem of the SMR process is carbon formation because the process operates at temperatures above 800 °C, which is over the temperature that favours the hydrocarbon cracking reactions (620 °C). Simultaneously with carbon formation, carbon gasification reactions remove the carbon laid down, reducing the net accumulation of carbon in a well-run process. The rate of carbon formation depends on several conditions, like catalyst activity and heat flux, which may be varied in order to change the ratio of carbon formation/gasification to minimise its accumulation (Carlsson, 2015).

2.1.2 Catalysts

A number of catalysts containing both noble and transition metals have been studied. Group VIII metals, such as iron, as well as nickel and cobalt, are active for the steam reforming reaction (Rostrup-Nielsen, 2008). Nickel is usually the chosen one, since cobalt is oxidized under normal reforming conditions and iron requires a strongly reducing atmosphere (Rostrup-Nielsen, 2008).

Catalysts based on Ni have been found to have high catalytic activity and high selectivity for SMR. As disadvantages, they have a high carbon deposition rate and suffer sulphur poisoning and sintering. The coking resistance of the Ni catalyst can be improved by the addition of small amount of noble metals, rare earth metals and supporting material, like perovskites, producing affordable catalysts with good catalytic properties and low carbon sensibility.

Lately, the carbon deposition problem is being addressed through the development of more active and stable catalysts with different combinations of metals (Ni, Pt, Ru, Rh) and support ($La_2Zr_2O_7$, Al_2O_3, CeO_2), usually prepared through impregnation. Table 2-2 summarizes some of the latest created catalysts (Sengodan et al., 2018).

Table 2-2. Recently developed catalysts for the SMR reaction (Sengodan et al., 2018).

Catalyst	H_2O/CH_4 ratio	*T* (°C)	CH_4 conv. (%)	Reference
$Ni/\gamma\text{-}Al_2O_3$	3	655	88	(Kim et al., 2015)
$Ni\text{-}Rh/Al_2O_3$	3	800	32.2	(Luna et al., 1999)
$Ru/MgO\text{-}Nb_2O_5$	4	700	>95	(Amjad et al., 2015)
Rh/CeO_2	1.2	800	99.4	(Vita et al., 2015)

2.1.3 Steam reforming reactor

Steam Reforming is, in industrial practice, mainly carried out in reactors referred to as steam reformers, which are essentially fired heaters with catalyst-filled tubes placed in the radiant part of the heater. The process may also be carried out in reactors referred to as heat exchange reformers (Aasberg-Petersen et al., 2004). Figure 2-1 shows two examples of such reactors.

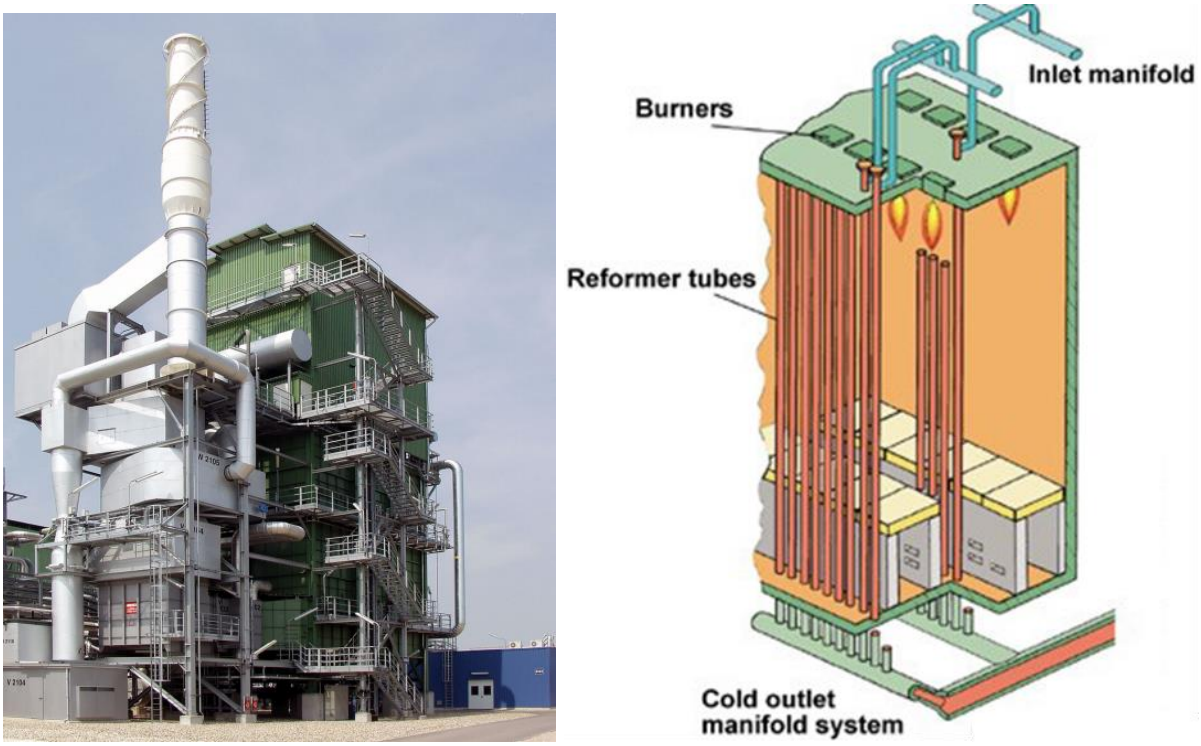

Figure 2-1. Conventional Linde Engineering steam reformer (left) (Linde Engineering, 2018) and the proprietary Uhde top-fired steam reformer (right) (thyssenkrupp, 2018).

A conventional methane steam reformer reactor has two main parts: the tubes and the furnace. While the reforming reaction occurs inside the multiple parallel tubes containing a nickel catalyst, the heat required for the endothermic reaction of reforming is generated in the outer side of the tubes by burning fuel in the furnace. Different tube wall temperature and heat flux

profiles result from various firing arrangements in the reformer furnace, being the most common the bottom fired, top fired, side fired and terrace wall (Zamaniyan et al., 2008).

In the reformer itself, the primary heat transfer mechanism is radiation and, within the tube, it is convection and conduction, being the internal wall the hottest point inside the tube. The presence of hot spots and temperature gradients inside the tubes are the two main problems of the steam reformer configuration, since higher temperature zones increase the probability of carbon formation.

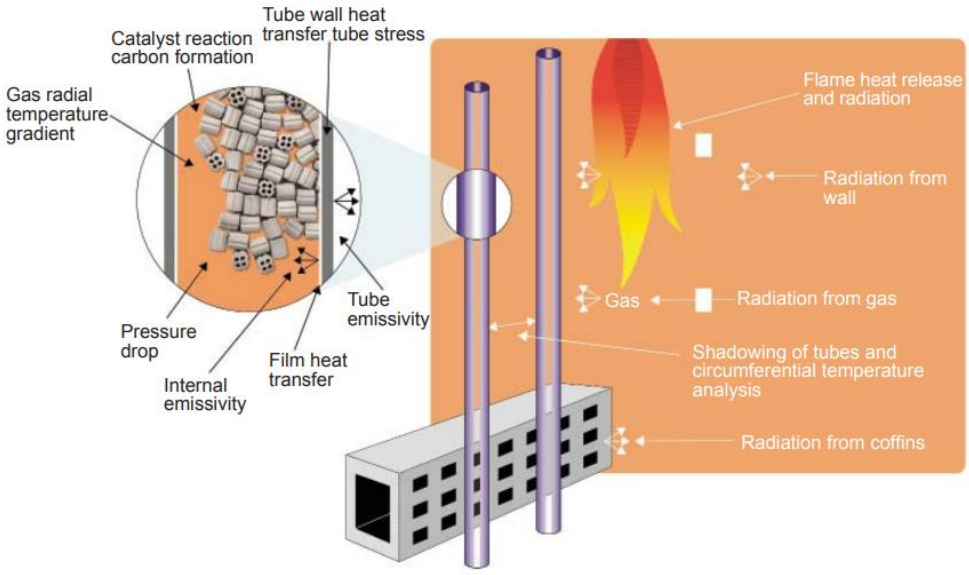

Figure 2-2. Heat transfer balance inside a steam reformer (Carlsson, 2015).

Another problem of the steam reforming in fixed-bed tubes is that the reforming reaction is diffusion limited, which can be minimized by using a higher surface area catalyst. Besides catalyst activity, catalyst size and shape is also important, since it has an impact on the tube-side laminar film layers and therefore, in the overall heat transfer coefficient, decreasing the inside tube wall temperature and influencing the carbon formation and the methane conversion (Carlsson, 2015).

2.1.4 SMR typical industrial plant

The first step of the SMR process is desulphurization of the natural gas feed. The catalyst used in the reforming process is highly sensitive to any sulphur compounds, therefore these compounds need to be reduced to a usual concentration of less than 0.15 mg $S \cdot m_N^{-3}$. The feed gas is preheated up to 350-400 °C, the sulphur compounds are hydrogenated to H_2S and then finally adsorbed on a ZnO bed.

Next, the gas feed is mixed with steam and enters the pre-reformer at a temperature around 400-600 °C, reacting according to Equation 2.1. The applied steam to carbon ratio is typically 3, although the actual optimum ratio depends on several factors (such as feedstock quality, purge gas recovery and shift operation). The use of a pre-reformer allows to reduce the size of the main reformer, decreasing operating costs due to savings in fuel consumption (Johnson Matthey, 2018). Typical methane conversion is around 60 %. Because the reforming reaction is endothermic, the reaction heat and the required temperature are obtained through internal combustion of part of the reaction feed gas, prior to its injection in the main reformer tubes filled with catalyst. The main reforming results in a gas outlet temperature around 900 °C, before being cooled down to 330-380 °C.

The CO still in the process gas from the tubular reformer is converted to CO_2 and H_2, in the shift section, according to Equation 2.2. The water-gas shift reaction is carried out in two steps and is described with more detail in Appendix A. After the shift section, the CO_2 still present in the syngas is removed in a chemical or physical absorption process. Finally, the final hydrogen stream can go through a pressure swing adsorption unit to be purified (European Commission, 2007).

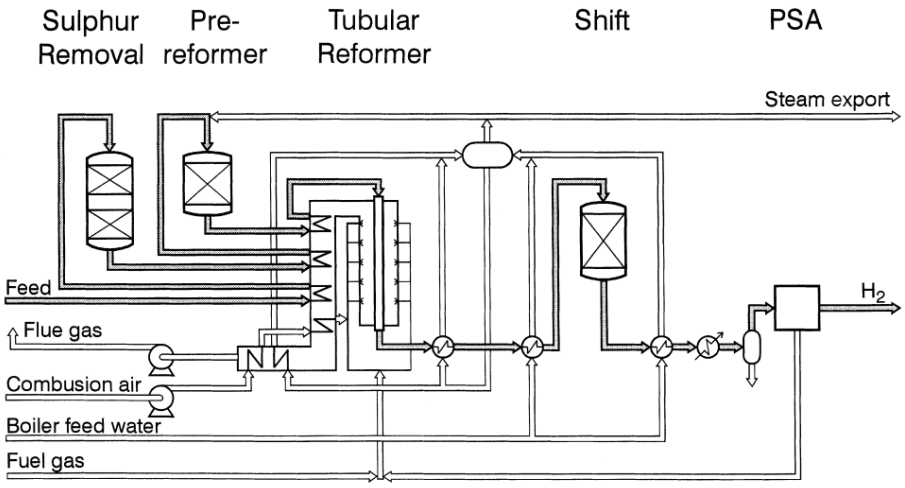

Figure 2-3. Typical process layout for a Haldor Topsøe hydrogen industrial plant based on advanced tubular steam reforming technology (Aasberg-Petersen et al., 1998).

2.1.5 State of the art technology

Several companies have been developing micro/mini structured SMR reactors to minimize mass and heat transfer problems associated to the typical fired reformer configuration. The leading companies are CompactGTL and Velocys©, whose SMR reactors are commercialized for GTL (Gas-to-Liquids) plants.

CompactGTL is the world's largest small scale, modular GTL company providing an end to end solution to the problem of associated and stranded gas in oil and gas field development. Its modular Steam Methane Reforming reactor is in the form of a high temperature alloy brazed plate-fin unit, as can be seen in Figure 2-4. Every channel contains low pressure-drop catalyst coated metallic foil structures and there are two process streams in a co-linear flow configuration, a gas process stream and a combustion stream. The reactor works at 650-800 °C and at approximately 4 bar (CompactGTL, 2018).

Figure 2-4. CompactGTL modular SMR reactor configuration (CompactGTL, 2018).

CompactGTL modular SMR technology is ideally suited to offshore projects where it is not feasible to employ conventional SMR systems on floating production facilities (CompactGTL, 2018).

Velocys©, a spin-off of Battelle, is one of the pioneer organizations that demonstrated the concept of SMR in micro channel reactors. Velocys© employs a laminate or sheet construction technique for the microchannel reactor. The process consists of forming many parallel micro channels by interleaving (stacking) thin sheets of formed material (shims) with solid sheets (walls) (Tonkovich et al., 2005).

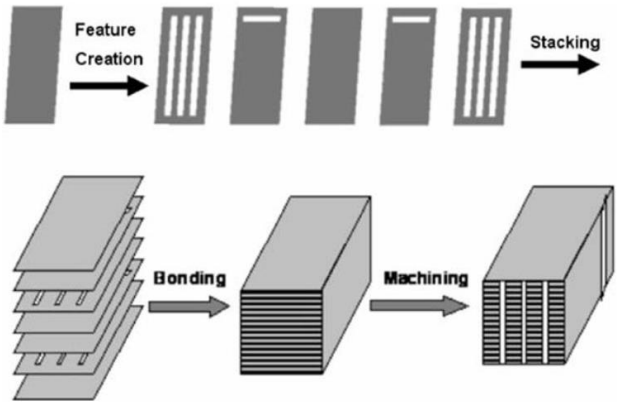

Figure 2-5. Manufacturing steps to produce microchannel reactors (Tonkovich et al., 2005).

Figure 2-6 shows one of the first SMR micro reactors built by Velocys©. It consists of more than 500 shims of roughly 30 cm by 38 cm. The stack height is 30 cm and each shim is made from In617 (Tonkovich et al., 2005).

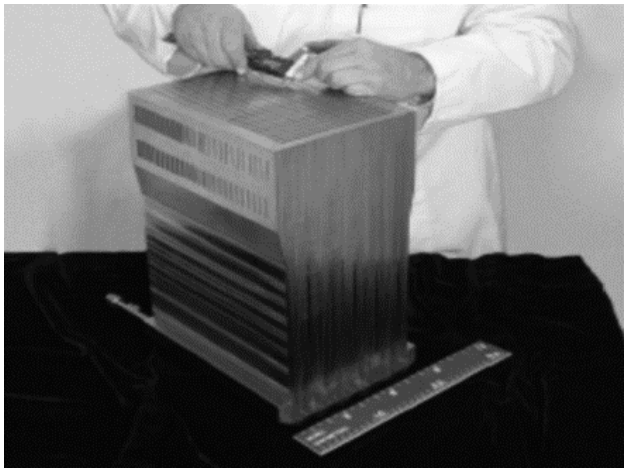

Figure 2-6. Velocys© microchannel device (Tonkovich et al., 2005).

As can be seen in Figure 2-7, the input streams – fuel, air, and reactant (methane and steam) – enter the device at one end, the cold end, to minimize thermal strain during operation. All streams undergo a U-bend at the hot end of the reactor. Fuel and air enter the reactor at the device cold end through a macro-to-micro manifold (Tonkovich et al., 2004). This manifold then distributes the flow into the individual micro channels. The air micro channels further mix air into the fuel channels to initiate the combustion reaction that supplies heat to the adjacent SMR reactor micro channels. The exhaust micro channels collect the combustion product stream and remove the fluid from the reactor. The reaction zone, where the catalyst is located (light grey rectangle), resides at the hot end of this arrangement. In this manner there is an intensive heat recovery between the fresh cold streams entering the system and the exhaust streams leaving the system.

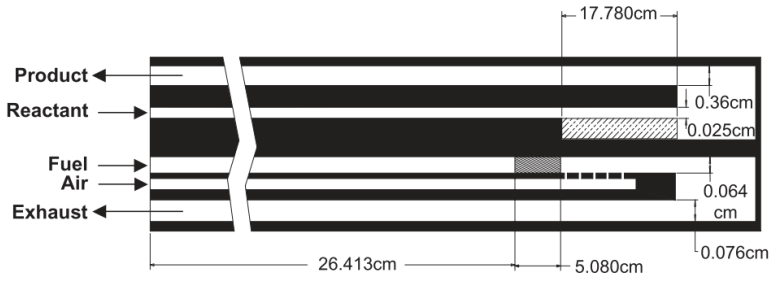

Figure 2-7. SMR and combustion flow arrangements (Tonkovich et al., 2004).

Velocys© has reported tests of SMR micro reacting systems, ranging from single channel systems to full scale systems, with syngas production of 360–800 $m_N^{-3} \cdot h^{-1}$, with the larger tested system achieving about 1000 hours on-stream (Zanfir, 2014).

2.2 The NETmix® technology

The NETmix® technology, developed at LSRE-LCM, is a patented technology (Lopes et al., 2005), initially registered by Universidade do Porto, and now owned by Fluidinova. Its characteristic geometry, consisting on a network of mixing chambers interconnected by transport channels, allows mixing fluids in a controlled way without using external mechanical mixing equipment (Gomes, 2011). Figure 2-8 presents a NETmix® network and its unit cell.

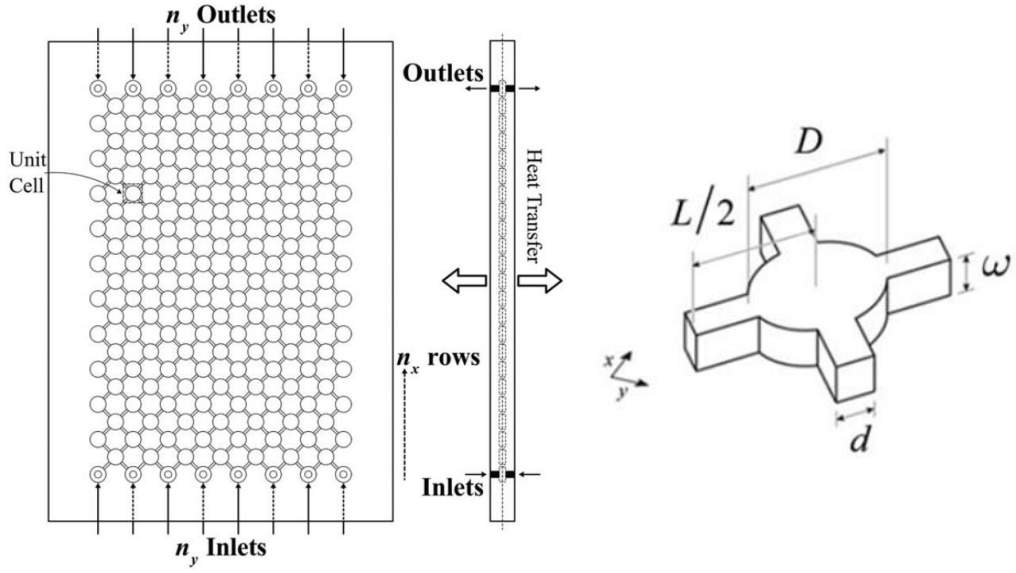

Figure 2-8. Front and side-view drawing of a NETmix® network (left) and a NETmix® unit cell (right). (Costa et al., 2017)

The regular network is generated by repetition of a unit cell organized into consecutive pairs of n_x rows, with n_y and $n_y - 1$ number of cells, and the device is open to flow through equal number, n_y, of inlets and outlets. Each unit cell is composed by one cylindrical chamber and two inlet and two outlet rectangular half-channels oriented at a 45º angle from the main flow direction. (Laranjeira, 2005) The network can be easily scaled-up or numbered-up depending on the process and production objectives.

In the present work, the reactor considered is the LabNETmix reactor, which has the geometry presented in Figure 2-8 and the dimensions listed in Table 2-3. For application of this technology to SMR, in addition to the reaction plates, there is the need for plates where combustion of methane occurs to supply heat for the reaction.

Table 2-3. LabNETmix dimensions.

d (mm)	1
ω (mm)	3
D (mm)	6.5
L (mm)	8.5
n_x	29
n_y	8

Proper mixing in a NETmix® network can only be achieved above the critical channel's Reynolds number (ratio between inertial and viscous forces), from which the flow inside the chambers changes from a fully developed laminar parallel flow to a self-sustained dynamic and chaotic oscillatory flow regime inducing strong laminar mixing. This phenomenon is attributed to the local hydrodynamic instabilities induced by geometric characteristics and by the impinging jets interactions within the chambers (Laranjeira et al., 2009). NETmix® is a mixing device particularly suited to handle reactions where fast interfacial mass transfer is required, such as heterogeneous catalytic and gas-liquid reactions, since its mixing mechanisms enhance the production of significant interfacial area, thus improving mass transfer.

Besides high mass transfer rates, NETmix® has a great ability to remove or absorb heat due to its high surface to volume ratio, in the order of 10^3 m^2/m^3 (Fonte, 2013). Figure 2-9 compares the specific heat transfer capacity of NETmix® with several commercially available technologies, which can be 2 to 5 orders of magnitude higher than most of the technologies used industrially and nearly one order of magnitude larger than micro reactors. Thus, the NETmix® technology is a good candidate for solving the major mass and heat transfer problems that exist in the conventional steam methane reforming processes (Costa et al., 2017).

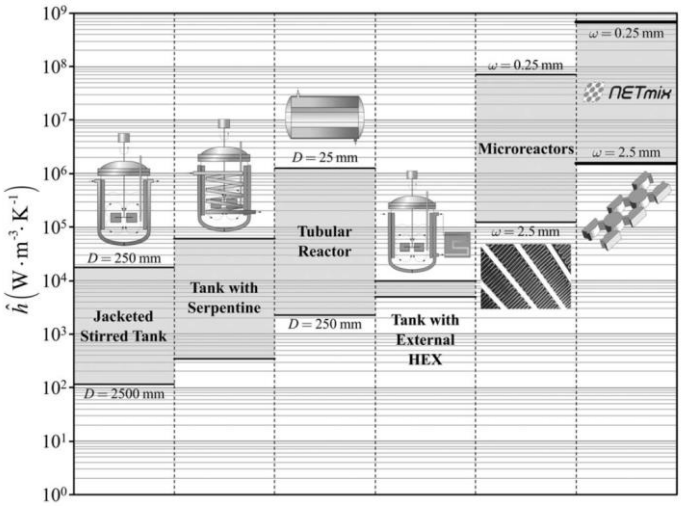

Figure 2-9. Specific heat transfer capacity of typical equipment (Costa et al., 2017)

3 Steam Methane Reforming catalyst studies

In this chapter, a rhodium-based catalyst for SMR developed by Velocys©, former Oxford Catalysts, is presented and the introduction of its associated kinetics in a simulation software is validated against experimental data. The adaptation of the rhodium supported catalyst to a thin layer of rhodium catalyst applied by sputtering and the presence of mass diffusion limitations, when the new catalyst is used in the LabNETmix reactor, are also studied.

3.1 Velocys© microchannel reactor for SMR

Besides activity and stability studies for a rhodium-based catalyst (Wang et al., 2004), whose preparation is described in Appendix B, experimental and modelling studies of the catalyst performance in a single channel micro reactor can be found in the literature (Tonkovich et al., 2007).

The single channel micro reactor used to test the rhodium-based engineered catalyst in industrial conditions is built from Inconel 625 (a nickel-based super alloy that exhibits high oxidation, corrosion and temperature resistance) (Rickard Specialty Metals & Engineering, 2013) and includes a single long open reactor channel, where the reforming reaction takes place, and several adjacent and perpendicular channels, where a combustion reaction provides enough heat for the endothermic reforming process. Figure 3-1 shows a scheme of the reactor operated by Tonkovich et al., 2007.

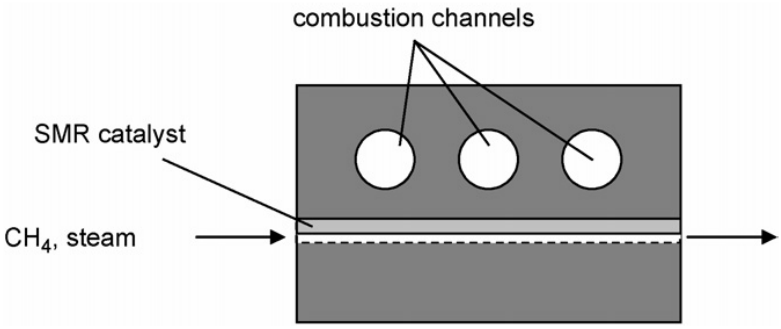

Figure 3-1. Schematic of experimentally tested single micro channel (Tonkovich et al., 2007).

The single channel is 11.4 mm long, 10.7 mm wide and has 356 µm open gap. As can be seen on the scheme, the engineered catalyst, which is 280 µm thick, is cut with the same dimensions and is supported on the heat transfer wall by two Inconel strips of metal along the sides of the catalyst insert. This felt is loaded with 12.5 mg of rhodium catalyst. A mixture of methane and steam is fed to the single channel while a mixture of hydrogen and air is fed to the combustion channels.

3.2 SMR kinetics

In agreement with Tonkovich et al., 2007, and since the focus of this study is the methane reforming reaction in a microchannel reactor, the main reactions to consider are the SMR reaction and the WGS reaction (which also occurs on the rhodium catalyst), already presented in Section 2.1.1., and represented by Equations 2.1 and 2.2, respectively.

The reaction rate, rate constants and equilibrium constants of both reactions are given by the following equations:

$$r_1 = k_1 \left(p_{CH_4} p_{H_2O} - \frac{p_{CO} p_{H_2}^3}{K_1} \right) \quad (3.1)$$

$$r_2 = k_2 \left(p_{CO} p_{H_2O} - \frac{p_{H_2} p_{CO_2}}{K_2} \right) \quad (3.2)$$

$$k_1 = A_1 \exp\left(-\frac{E_1}{RT}\right) \quad (3.3)$$

$$k_2 = A_2 \exp\left(-\frac{E_2}{RT}\right) \quad (3.4)$$

$$K_1 = \exp\left(\frac{-26\,830}{T} + 30.114\right) \quad (3.5)$$

$$K_2 = \exp\left(\frac{4\,400}{T} - 4.036\right) \quad (3.6)$$

where r_i is the reaction rate of the reaction i, k_i is the kinetic rate constant of the reaction i, p_j is the partial pressure of the component j, K_i is the equilibrium constant for the reaction i (K_1 is in bar^2 and K_2 is dimensionless), A_i is the pre-exponential factor for the reaction i, E_i is the activation energy for the reaction i and T is temperature. Here, i = 1 refers to the SMR reaction and i = 2 to the WGS reaction. The value of the kinetic parameters for Equations 3.1 to 3.6 are given in Table 3-1 .

Table 3-1. Kinetic parameters.

A_1 (kmol·m$^{-3}_{cat}$ s^{-1} bar^{-2})	1.28x10^8
A_2 (kmol·m$^{-3}_{cat}$ s^{-1} bar^{-2})	1.47x10^3
E_1 (J·kmol^{-1})	1.70x10^8
E_2 (J·kmol^{-1})	6.71x10^7

3.3 Kinetic model validation methodology

To validate the kinetic model, it was decided to study the microchannel reactor performance in Aspen Plus® V9, a simulation software from AspenTech®, to compare the experimental results

with the modelled results from the software. Aspen Plus® is particularly designed for bulk, speciality chemical and pharmaceutical industries to optimize throughput, quality and energy use. The thermodynamic method applied is Peng-Robinson equation of state with Boston-Mathias modifications, recommended for gas processing and petrochemical applications (Technology, 2001).

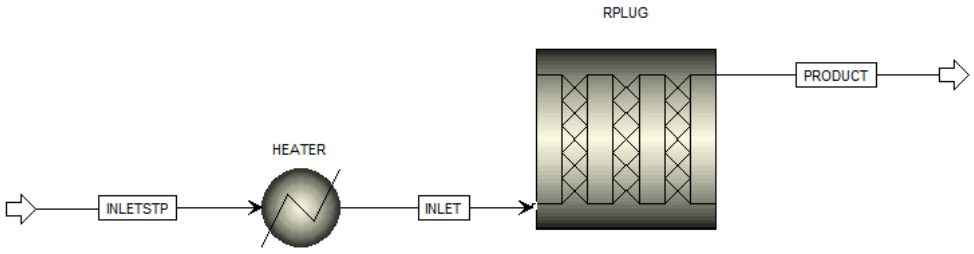

Figure 3-2. Layout for the microchannel reactor simulation in Aspen Plus®.

First, the layout used for the simulation is defined. A HEATER block is used to convert the INLETSTP stream units given by the paper studied (Tonkovich et al., 2007) from SLPM (standard litres per minute), at 0 °C and 1 atm, to the reactor operation conditions presented in Table 3-4. The RPlug block model is used to model the single microchannel, since the flow patterns in the latter can be conceptualized as being plug flow, even though the flow is laminar. The inputs for this block are: length, catalyst mass, reaction kinetics, inlet flow rates and operating conditions. Since the microchannel is not cylindrical, the diameter was estimated assuming a cylindrical channel with the same 11.4 mm of length mentioned in Section 3.1 and maintaining the reaction volume and the residence time, thus giving an input of 2.2 mm for the diameter.

The engineered catalyst mass was calculated to be inserted in the program. Although the zeolite mass is referred in the literature, it was noticed that the kinetic equations depended on the catalyst volume. This catalyst volume includes the felt, since simulation runs assuming metal only did not return satisfying results. Given that, it was necessary to estimate the felt mass. Starting from its volume and density (0.36 $g \cdot cm^{-3}$) (Goodfellow, 2018), using a porosity of 0.5 (as assumed by Tonkovich et al., 2007), a felt mass of 12.3 mg was obtained. This resulted in a total mass of engineered catalyst of 24.8 mg.

Aspen's RPlug model only accepts mass-based kinetic expressions. Therefore, the kinetic rate constants had to be converted to adequate units ($kmol \cdot kg_{cat}^{-1} \cdot s^{-1} \cdot bar^{-2}$). To do so, the density of the catalyst is required and is estimated using the densities of both the zeolite and felt. To start with, the solid density, ρ_s, was obtained by a mass-weighted average of Rh, MgO and Al_2O_3 component densities. With that, and assuming an interparticle void fraction of 0.45, the zeolite density was calculated using:

$$\rho_z = \rho_s(1 - \varepsilon_z) \tag{3.7}$$

Finally, the whole catalyst density, ρ_{cat}, was obtained through another mass-weighted average using the mass fractions and porosities of the zeolite and felt, resulting in a final density of 1.51 g·cm^{-3}. Table 3-2 summarises the catalyst parameters considering the felt.

Table 3-2. Catalyst parameters (with felt).

$\boldsymbol{\rho_f}$ **(g·cm^{-3})**	0.36
$\boldsymbol{\rho_z}$ **(g·cm^{-3})**	2.36
$\boldsymbol{\rho_{cat}}$ **(g·cm^{-3})**	1.51
$\boldsymbol{\varepsilon_{cat}}$	0.5
Mass (mg)	24.8

The new kinetic parameters, now depending on the catalyst mass, were calculated for both direct and reverse reactions and are presented on Table 3-3, as well as the activation energies. The reverse kinetic parameters were obtained knowing that the equilibrium constant corresponds to ratio of the reaction of the forward reaction rate and the reverse reaction rate.

Table 3-3. Mass-dependent kinetic parameters.

$\boldsymbol{A_1}$ **(kmol·kg$^{-1}_{cat}$ s^{-1} bar^{-2})**	8.46x10^{4}	$\boldsymbol{E_1}$ **(J·kmol^{-1})**	1.70x10^{8}
$\boldsymbol{A_1'}$ **(kmol·kg$^{-1}_{cat}$ s^{-1} bar^{-2})**	7.07x10^{-9}	$\boldsymbol{E_1'}$ **(J·kmol^{-1})**	-5.35x10^{7}
$\boldsymbol{A_2}$ **(kmol·kg$^{-1}_{cat}$ s^{-1} bar^{-2})**	9.73x10^{-1}	$\boldsymbol{E_2}$ **(J·kmol^{-1})**	6.71x10^{7}
$\boldsymbol{A_2'}$ **(kmol·kg$^{-1}_{cat}$ s^{-1} bar^{-2})**	55.1	$\boldsymbol{E_2'}$ **(J·kmol^{-1})**	1.04x10^{8}

The inlet flow rates and the operation conditions were defined to match two experimental cases studied by Tonkovich et al., 2007. The inlet flow rate was set to give the contact times (defined as the catalyst bed volume divided by the volumetric inlet gas flow rate at STP conditions) of 900 μs and 90 μs. The operation conditions are summarised in Table 3-4.

The results obtained after simulating both cases are summarized in Table 3-5. The molar conversion of CH_4 is calculated through Equation 3.8 (Tonkovich et al., 2007), the equilibrium conversion is obtained through a simulation with a REquil block in Aspen Plus®, which represents a rigorous equilibrium reactor based on stoichiometric approach, and the CO selectivity was calculated through Equation 3.9, where $y_{\mathrm{CO}}^{\mathrm{out}}$, $y_{\mathrm{CO_2}}^{\mathrm{out}}$ and $y_{\mathrm{CH_4}}^{\mathrm{out}}$ are the outlet molar fraction of carbon monoxide, carbon dioxide and methane, respectively, and $y_{\mathrm{CH_4}}^{\mathrm{in}}$ is the inlet molar fraction of methane.

Table 3-4. INLETSTP, INLET and reactor conditions (Tonkovich et al., 2007).

Contact time (μs)	900	90
Steam/CH_4 ratio	3	3
CH_4 flow (SLPM)	0.153	1.55
Steam flow (SLPM)	0.461	4.64
$T_{\text{in reactor}}$ (°C)	837	788
$T_{\text{out reactor}}$ (°C)	802	754
$P_{\text{in reactor}}$ (bar)	13.0	13.0
ΔP (bar)	0.1	0.9

Table 3-5. Performance results of Velocys© microchannel reactor for two different contact times.

	900 μs		90 μs	
	Aspen Plus®	(Tonkovich et al., 2007)	Aspen Plus®	(Tonkovich et al., 2007)
CH_4 conversion (%)	85.3	88.2	18.1	17.0
Eq. conversion (%)	95.3	89.1	93.3	86.4
S_{CO} (%)	41.3	38.3	58.8	43.0
Heat flux ($W \cdot cm^{-2}$)	16.6	18.9	31.8	21.3

$$X_{CH_4} = \left(\frac{y_{CO}^{out} + y_{CO_2}^{out}}{y_{CO}^{out} + y_{CO_2}^{out} + y_{CH_4}^{out}}\right) \times 100 \quad (3.8)$$

$$S_{CO} = \frac{y_{CO}^{out}}{y_{CH_4}^{in} - y_{CH_4}^{out}} \times 100 \quad (3.9)$$

Comparison between the simulated and experimental results is presented in Table 3-5. The values of CH_4 conversion and equilibrium conversion are the most similar ones, with absolute errors lower than 10 %. The differences observed might be related to the presence of heat and mass transfer limitations causing temperature and concentration profiles inside the catalyst (and throughout the reactor length) which are not accounted in the Aspen Plus® solution (Carberry, 1962). Also, the approximations made for the conversion of volume-based kinetics to mass-based kinetics, and the assumption that the total engineered catalyst and felt mass are available for the reaction might have introduced additional deviations. Nevertheless, the deviations are small and it can be concluded that the experimental results reported in

Tonkovich et al., 2007 are well reproduced through simulation, using the reported kinetics, within a 10 % error. Therefore, this simulation procedure can be used as a starting point for modelling a LabNETmix reactor for SMR.

3.4 Application by sputtering

Instead of using the supported Velocys© rhodium-based catalyst, the catalyst concept chosen for the LabNETmix was a thin layer of rhodium applied by sputtering deposition onto the surface wall of the reactor (one layer on the top wall and another on the bottom wall), which allows a high reaction extent without compromising heat and mass transportation. Figure 3-3 presents a scheme of a layer of rhodium and its arrangement in the NETmix® unit cell.

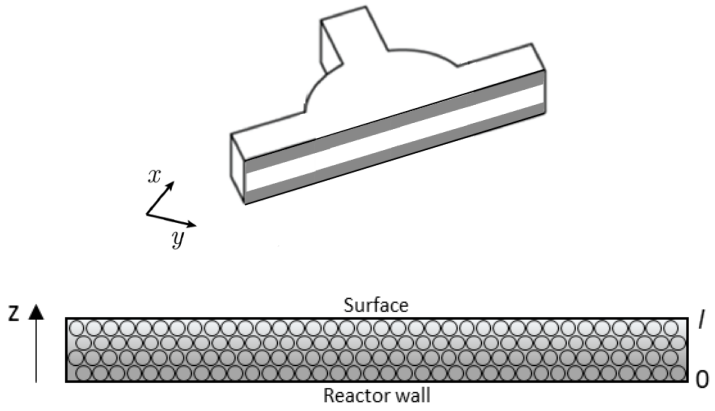

Figure 3-3. Cut of the two layers of sputtered rhodium in the reactor plate (up) and detail of the rhodium thin layer (down).

Sputtering is, on an atomic level, the process whereby atoms are ejected from a target (in this case is rhodium) that is to be deposited on a substrate (the reactor walls) as a result of the bombardment of the Rh target by high energy particles. The substrate is placed in a vacuum chamber containing an inert gas – usually Argon – and a negative charge is applied to the target material that will be deposited onto the substrate, causing the plasma to glow. (Hughes, 2014)

The well-packed layers of rhodium studied are 200 nm thick (l), each, and they are composed by grains with 50 nm of diameter (Orlinski et al., 2000) and with a crystallite size of about 10 nm. (Marot et al., 2007). Because the catalyst does not have a support, unlike Velocys© engineered catalyst, the prior kinetic expressions cannot reproduce the catalyst performance. Therefore, an adaptation based on the active metal mass is required. The calculation is described in detail in Section 3.5.

3.5 Mass diffusion limitations/ internal mass transfer limitations

The existence of mass diffusion limitations was studied for the sputtered layers of rhodium catalyst considering a void fraction of 0.5 and an operating temperature of 837 °C, retrieved from Velocys© work. The pressure in the single LabNETmix plate studied was maintained at 13 bar. The examined parameters were the Thiele modulus and the effectiveness factor.

In the present work, and for simplification purposes, the main focus is the study of methane diffusivity problems. It is assumed that steam is in excess (steam to methane molar ratio of 3:1) and that the system is far from equilibrium, which resulted in the following irreversible reaction:

$$\mathrm{CH_4 + H_2O \rightarrow CO + 3H_2} \tag{3.10}$$

$$r_1 = k_1 p_{\mathrm{CH_4}} p_{\mathrm{H_2O}} \tag{3.11}$$

First, using the grain diameter and assuming spherical particles, the volume of the total spheres in one layer and the bed volume is estimated. From the bed volume and rhodium density (12.41 g·cm^{-3}) (The National Institute for Occupational Safety and Health, 2016), it was obtained 9.99 mg of rhodium per layer with a specific area of 12.9 m^2·g^{-1} and a tortuosity of 0.707 (square-root of porosity).

Next, it was necessary to adapt Equation 3.1 by eliminating the factor that concerns equilibrium, resulting in Equation 3.11. After, the pre-exponential factor A_1 is corrected considering that, for the same mass, the sputtered catalyst has 10 times more active metal than the supported Velocys© catalyst, since the rhodium mass percentage increases from 10 %, in the case of Velocys© catalyst, to 100 %. Therefore, since the kinetic rate directly depends on the catalyst mass, the new pre-exponential factor is 1.28x10^9 kmol·m$^{-3}_{cat}$·s^{-1}·bar^{-2} (2.05x10^5 kmol·kg$^{-1}_{cat}$·s^{-}·bar^{-2}). This value is only applicable when considering an ideal case in which the increase of active centres is directly proportional to the increase of mass and that all of them are equally accessible by the reactants.

For the purpose of calculating the molecular diffusion coefficient for methane gas at 13 bar, the theoretical method of Chapman-Enskog was employed. (Cussler, 2009)

$$\mathcal{D} = \frac{1.86\times10^{-3} T^{2/3} (1/\widetilde{M}_1 + 1/\widetilde{M}_2)^2}{P\sigma_{12}^2 \Omega} \tag{3.12}$$

$$\sigma_{12}^2 = \frac{1}{2}(\sigma_1 + \sigma_2) \tag{3.13}$$

where $\mathcal{D}$ is the molecular diffusion coefficient, T is the absolute temperature, P is the pressure in atmospheres and $\widetilde{M}_j$ is the molecular weight of component j. The quantities σ_{12}, collision diameter, and Ω, the dimensionless collision integral, are molecular properties characteristic of the detailed theory. Considering just one species, both 1 and 2 correspond to methane. For

a temperature of 837 °C, retrieved from Velocys© work and used throughout the cases studied, the diffusivity of methane is 7.45×10^{-5} $m^2 \cdot s^{-1}$.

Next, the contribution of the molecular and the Knudsen diffusions, $\mathcal{D}$ and $\mathcal{D}_k$, respectively, was evaluated. For a pore size of 20 nm (Chung et al., 2013), i.e., mesopores according to IUPAC classification (Zdravkov et al., 2007), the Knudsen diffusion, given by the kinetic theory of gases (Equation 3.14), occurs when the mean free path is relatively long compared to the pore size, so the molecules collide frequently with the pore wall.

$$\mathcal{D}_k = \frac{4}{3} r' \sqrt{\frac{2}{\pi} \frac{RT}{\widetilde{M}}} \tag{3.14}$$

$$m = \frac{k_B T / P}{\left(\frac{\pi}{4}\delta^2\right)} \tag{3.15}$$

where r' the pore radius, R is the universal gas constant in, $\widetilde{M}$ is the molecular weight, m is the mean free path, k_B is the Boltzmann constant, P is the absolute pressure in Pa and δ is the diameter of the sphere.

The Knudsen diffusion has a greater influence in the combined diffusivity in the catalyst pores because the pore size is smaller than the mean free path of the methane molecules calculated from the kinetic theory of gases (106 nm). Finally, the effective diffusivity is found to be 5.15×10^{-6} $m^2 \cdot s^{-1}$.

After the diffusivity is determined, the next step is to perform a Thiele modulus analysis to assess internal mass transfer limitations. For this, slab geometry, isothermal profiles and a pseudo first order reaction are considered. A first order reaction can be assumed given the excess of steam and the assumption that the system is far from equilibrium, as previously mentioned. The normalized mass balance equation that describes mass transfer inside the catalyst thin layer, under these assumptions, is given by:

$$\frac{\mathrm{d}^2 f_{\mathrm{CH_4}}}{\mathrm{d}x^2} - \Phi^2 f_{\mathrm{CH_4}} = 0 \tag{3.16}$$

where $f_{\mathrm{CH_4}}$ is the methane concentration, normalized by the surface concentration; x is the position in the layer, normalized by the layer thickness, l, and Φ is the Thiele modulus, which is defined as:

$$\Phi = \sqrt{\frac{k_1 l^2 \, C^S_{\mathrm{H_2O}} (RT)^2}{D_{eff}}} \tag{3.17}$$

Deduction of Equation 3.16 and Equation 3.17 is described in detail in Appendix C. The surface concentration values used were estimated through a simulation in Aspen Plus® using the same flowsheet from Figure 3-2. This approach has the drawback of not considering eventual mass transfer limitations. Solving the second order differential equation with a RK23 algorithm

method, assuming $\mathrm{d}f_{CH_4}/\mathrm{d}x = 0$, when $x = 0$, and $f_{\mathrm{CH_4}} = 1$, when $x = 1$, as boundary conditions, the concentration profile inside the slab was obtained.

$$f_{\mathrm{CH_4}} = \frac{\cosh(\Phi x)}{\cosh(\Phi)} \tag{3.18}$$

$$\eta = \frac{\tanh(\Phi)}{\Phi} \tag{3.19}$$

The effectiveness factor, η, deducted in Appendix C and given by Equation 3.19, represents how far the observed reaction rate, calculated by the Gauss Theorem, is from the true reaction rate if the whole catalyst was at surface conditions. Figure 3-4 is the graphical representation of the methane concentration profile inside the catalyst layer and Table 3-6 presents the obtained values for the Thiele modulus and the effectiveness factor.

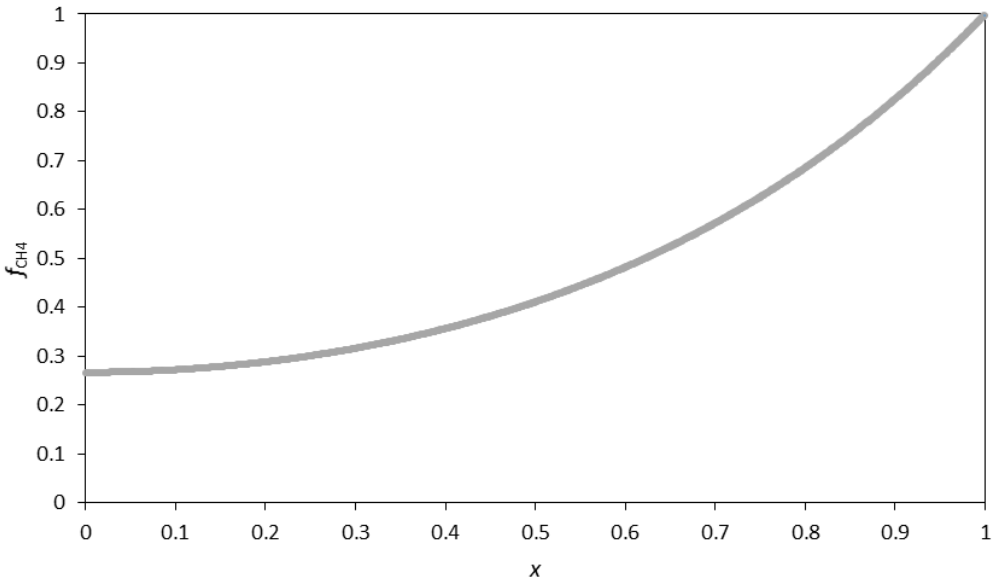

Figure 3-4. CH_4 concentration profile (normalized) inside the catalyst layer.

Table 3-6. Studied parameters for a 200 mm layer.

$\boldsymbol{\Phi}$	2.00
$\boldsymbol{\eta}$	0.483

From Figure 3-4 and Table 3-6, it is possible to verify that the particle is operating within the intermediate regime. The methane concentration profile inside the slab is accentuated and has a minimum value of 0.267 near the reactor wall, which confirms that the diffusion of methane to the centre of the catalyst is slower than the chemical reaction. Also, based on the expression for the effectiveness factor, when the Thiele modulus is between 1/3 and 3 (from the asymptotic expression of η for a slab), it is in intermediate regime and means that only 48.3 % of the slab is being used, which means that, in a real case, more catalyst is needed to achieve the same results.

In order to assess the impact of the approximations made to adapt the kinetic constants, a sensitivity analysis is performed by increasing and decreasing the value of the pre-exponential factor A_1, which directly affects the Thiele modulus. It was found that the intermediate regime changes to diffusional regime ($\Phi > 3$) when the kinetic rate is increased by 150 % and that, even if the kinetic expression had not been updated, the system would be on the limit of chemical regime ($\Phi \approx 1/3$). Thus, even if the updated kinetics don't correspond to the reality of increasing the active metal percentage on the catalyst, a substantial deviation on the pre-exponential factor is needed to change the system behaviour.

To confirm the presence of mass transfer problems in the Velocys© catalyst and to compare it with the sputtered Rh catalyst, the same methodology is used. The resulting parameters are presented in Table 3-7, which confirm that the catalyst is in the diffusional regime (the Thiele modulus is greater than 3).

Table 3-7. Studied parameters for Velocys© catalyst.

$\boldsymbol{\Phi}$	21.5
$\boldsymbol{\eta}$	4.65×10^{-2}

Thus, the adapted catalyst, a layer of rhodium, has a better performance than Velocys© catalyst if both were applied to the LabNETmix, decreasing the mass diffusivity problems encountered in the supported catalyst.

4 Simulation of Steam Methane Reforming on LabNETmix

In this chapter, an industrial plant of SMR with a scaled-up LabNETmix device as the SMR reactor is simulated using Aspen Plus®, and its flowsheet is explained in detail. Also, an estimation of CAPEX and OPEX is presented.

4.1 Aspen Plus® simulation of an industrial plant

The work from Carrara et al., 2010 was chosen as a guide for the operational conditions and process units usually encountered in a common industrial hydrogen plant. This work describes an Aspen Plus® simulation of a steam reforming industrial plant to evaluate its energetic performance. Figure 4-1 shows the process diagram of the reference plant SIAD S.p.A., located in the north of Italy.

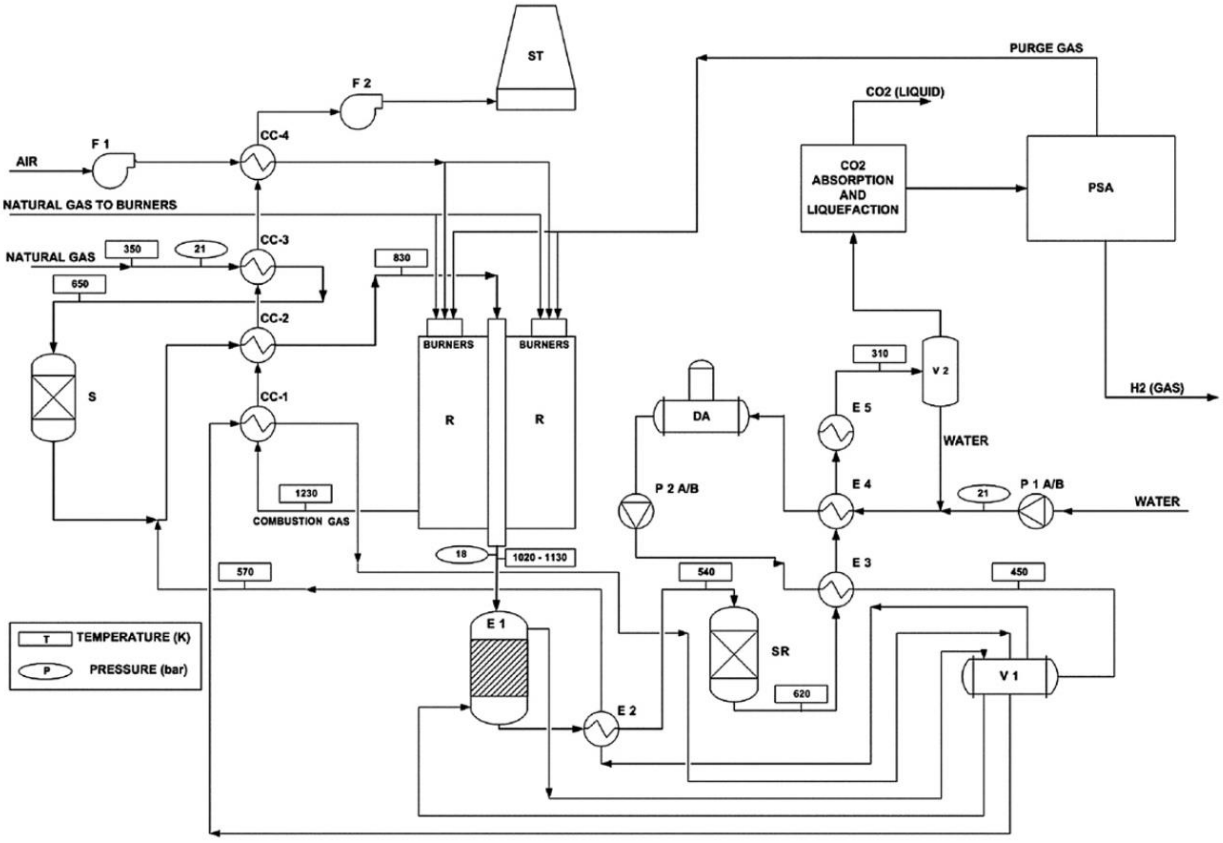

Figure 4-1. Reference plant layout (CC: combustion gas coolers (CC-1: steam boiler); DA: de-aerator; E: process gas coolers (E1: steam boiler); F: fans; P: pumps; R: Reformer; S: sulfur removal unit; SR: shift reactor; ST: stack; V1: steam drum; V2: water separation unit) (Carrara et al., 2010).

Unlike the plant represented in Figure 4-1, the main purpose of the simulated industrial plant is not the production of hydrogen from natural gas but the production of syngas with a H_2/CO molar ratio of 2 to be used as a feedstock for a Fischer-Tropsch industrial plant producing 250 barrels per day (1 oil barrel = 159 L). If produced in excess, the remnant hydrogen can be purified and sold for other applications such as turbines or fuel cells.

As a first approach, the process represented in from Figure 4-1 was reproduced in Aspen Plus®, apart from the reformer (R) and the shift reactor (SR), which were replaced by a scaled-up LabNETmix reactor. It is assumed in the present work that both processes occur in the same unit. Also, the CO_2 absorption and liquefaction units were replaced by a PSA (pressure swing adsorption) unit. The final layout, presented in Figure 4-2, was created by adapting the reactant flow rates and the operating conditions to obtain a CH_4 conversion higher than 75 %. To model the industrial plant, Peng-Robinson's thermodynamic property method was chosen.

4.1.1 Natural gas pre-treatment

Natural gas feed composition presented in Table 4-1 (Carrara et al., 2010) is assumed in the present work, so that the streams response to temperature and pressure changes is as realistic as possible. Although the reforming of heavier hydrocarbons was not included in the kinetics studied, hydrocarbons heavier than methane were still considered in the simulation.

Table 4-1. Design natural gas composition.

Component	Molar concentration (%)
CH_4	96.34
C_2H_6	1.79
C_3H_8	0.41
n-C_4H_{10}	0.08
i-C_4H_{10}	0.06
n-C_5H_{12}	0.01
i-C_5H_{12}	0.01
C_6H_{14}	0.01
CO_2	0.09
N_2	1.19
He	0.01
S ($mg \cdot m_N^{-3}$ NG)	5

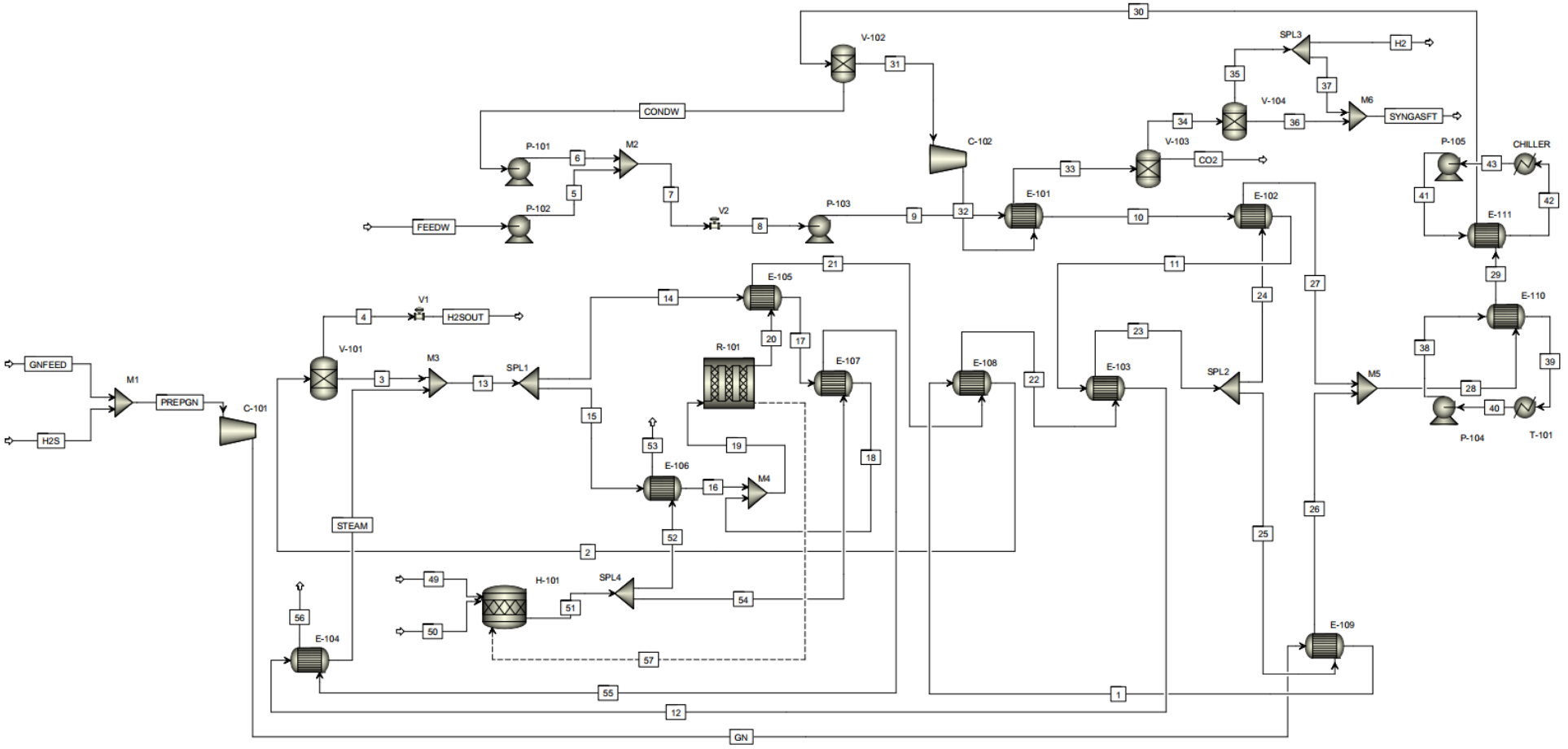

Figure 4-2. Aspen Plus® flowsheet of the SMR process with a LabNETmix reactor.

To better simulate an actual natural gas stream, which includes several sulphur compounds (responsible for poisoning the reforming catalyst), named here as PREPGN, two separate streams are combined:

- GNFEED, which comprises the components presented in Table 4-1 (apart from sulphur) and is considered to be fed to the process at approximate pipeline conditions (10 °C, 14 bar) (Zhao et al., 2014), although its final inlet temperature reaches 20 °C through due to heat transfer from ambient air;
- H2S, which represents the products resulting from the addition of H_2 to the natural gas stream, responsible for converting sulphur into H_2S, since solid sulphur is not adsorbed in the desulfurizer further ahead. It is important to highlight that this stream does not exist in a real plant, it was only created for calculation purposes.

Next, the 5.72 tonne·h^{-1} of hydrolysed natural gas are compressed to 21 bar using a centrifugal polytropic compressor with an ASME method for performance calculations and a polytropic and mechanical efficiencies of 76 % and 95 %, respectively. After, the natural gas is pre-heated to 377 °C by the hot gas products passing through two shell-and-tube heat exchangers, E-109 and E-108, before entering a packed tower working as a desulphurization unit, where H_2S in adsorbed in a ZnO bed (V-101). A process requirement is that the stream that feeds into the reactor R-101 must have less than 0.5 ppm of sulphur compounds, otherwise it will compromise the reforming catalyst, especially if it is nickel-based. To achieve that, the separation unit requires a 99.9 % efficiency, bringing the sulphur concentration down to 6.31×10^{-2} ppm, suitable for steam reforming and for sending the final product stream to either a cobalt or iron-based Fischer-Tropsch process (whose maximum sulphur limits are 0.1 and 0.2 ppm, respectively) (Khodakov et al., 2007).

4.1.2 Steam generation

Approximately 6.01 tonne·h^{-1} of fresh water is fed at a temperature and pressure of 14.9 °C and 1 bar, identified as FEEDW in Figure 4-2. Using a centrifugal pump with 63 % global efficiency (P-102), the water is pressurized to 21 bar before mixing it with another water stream (CONDW) resulting from a water separation unit (V-102) used in the separation and purification section.

The final stream, with 17.7 tonne·h^{-1} of water, is de-aerated (V2) (this unit is represented by a valve to account the pressure drop associated to the equipment) and pressurized again using a centrifugal pump (P-103) with 63.8 % efficiency to 26 bar. Afterwards, this water stream is heated to 297 °C (at these temperature and pressure conditions, the steam is in superheated conditions) before being mixed with the clean natural gas stream (stream 3).

The mass flow rate of fresh water introduced in the process through stream FEEDW is determined using a functionality available in Aspen Plus®, named *design spec*, where it is possible to determine a given value to achieve a certain goal. In the specific case of the present stream, the design spec is defined knowing that a molar H_2O/CH_4 ratio of 3:1 is required to guarantee a high methane conversion and to prevent the accumulation of solid carbonaceous products on the catalyst (the steam gasses the formed carbon/coke). The heat exchangers E-101, E-102, E-103 partially vaporize the water, increasing its temperature to 225 °C, while the heat exchanger E-104, a steam generator heated by combustion gases, completes the water vaporization and heats the steam to the desired 297 °C.

4.1.3 Reforming

The reforming section, unlike the reference plant, is only comprised by one reactor. In this case, and since the purpose of the simulated plant is to produce syngas and not H_2, the shift reactor was removed. This unit is responsible for converting CO into H_2, resulting in the increase of the H_2/CO final ratio, which is highly undesired in the present study.

An RPlug block is used to model the LabNETmix device. Although the technology is characterized by its unique mixing properties and quality (Costa et al., 2017), assuming plug flow is the most adequate model to simulate the global hydrodynamic behaviour of the device, since the global flow patterns are similar to a plug flow reactor with strong micro mixing. Also, the behaviour of the system approaches that of the PFR as the segregation parameter tends to one (ratio between the channels volume and the network volume, because the mixing of different streams only happens in the chambers) (Laranjeira, 2005).

The input parameters of the RPlug block are amongst others, the length and diameter. Since these parameters cannot be directly associated to NETmix® device dimensions, further calculations must be performed to better simulate the behaviour of the LabNETmix. To transform a 29 x 8 LabNETmix plate into one equivalent tubular reactor (instead of 14, the number of channels per row in the NETmix® reactor) it is necessary to calculate an equivalent diameter and length, considering that the new reactor is cylindrical and that it has the same volume has the original plate. A tubular reactor with 1.95×10^{-3} m of diameter and 8.05 m of length has the same volume and residence time of a LabNETmix plate. The scale-up of the tubular reactor can be performed in Aspen Plus® through the increase of the number of tubes.

Table 4-2. LabNETmix adapted dimensions used for modelling in Aspen Plus®.

Length (m)	8.05
Tube diameter (m)	1.95×10^{-3}
Number of tubes	70 455
Catalyst loading (kg)	1.41
Temperature (°C)	860
Pressure (bar)	20.1-19.1

The most important input parameter for the simulation is the catalyst loading, which is directly proportional to the number of tubes and significantly affects the reaction kinetics. Being that, to achieve a desirable methane conversion, the number of tubes is increased to 70 455, (equivalent to the same number of LabNETmix plates of 29 x 8 with two Rh sputtered layers with 200 nm thickness and to a reaction volume of 1.70 m^3) supporting 1.41 kg of rhodium.

To insert the kinetic expressions for the SMR and WGS reactions (direct and reverse equations had to be written separately) in Aspen Plus®, the pre-exponential factors had to be updated in the same way as it is done in Section 3.5 (because the catalyst is 100 % rhodium, more active metal means faster kinetics).

Table 4-3. Aspen Plus® input for SMR kinetic parameters.

A_1 (kmol·kg$^{-1}_{cat}$ s^{-1} bar^{-2})	2.05×10^5	E_1 (J·kmol^{-1})	1.70×10^8
A_1' (kmol·kg$^{-1}_{cat}$ s^{-1} bar^{-2})	1.72×10^{-8}	E_1' (J·kmol^{-1})	-5.35×10^7
A_2 (kmol·kg$^{-1}_{cat}$ s^{-1} bar^{-2})	2.36	E_2 (J·kmol^{-1})	6.71×10^7
A_2' (kmol·kg$^{-1}_{cat}$ s^{-1} bar^{-2})	1.34×10^2	E_2' (J·kmol^{-1})	1.04×10^8

Finally, the isothermal reforming reactor operating at 860 °C is capable of processing 23.4 tonne·h^{-1} of natural gas and steam, producing 5.57 tonne·h^{-1} of syngas (H_2 and CO only) with a methane conversion of 78 % and a weight fraction of unreacted methane of 5 %. To achieve this conversion and keep the temperature constant, 15.3 MW need to be provided to the reactor through combustion of natural gas (the reaction plates are intercalated with combustion plates).

4.1.4 Separation and purification

After cooling the reaction products (stream 20) by exchanging its heat with colder process streams (E-102, E-103, E-105 and E-109), the remaining heat is removed using cooling water

(E-110 and E-111). Cooling the product stream down to 30 ºC enables water condensation, resulting in stream CONDW that can be recycled at the beginning of the steam generation line.

After removing the water, the process stream is compressed to 33 bar using C-102, a centrifugal polytropic compressor using an ASME method for performance calculations and with a polytropic and mechanical efficiencies of 76 % and 95 %, respectively, and cooled down to 50 °C so it can be fed to the first of two pressure swing adsorption units. The first PSA unit, V-103, is responsible for cleaning the syngas by removing CO_2. The adsorption columns of the PSA cycle are not simulated because it is out of this work scope. Instead, the PSA process is represented by a separation block where CO_2 recovery is specified, based on literature results (94.2 %) (Ribeiro et al., 2012). The final CO_2 stream has a purity of 82.3 % and can be sent to a CO_2 capture unit while the remaining products go to a second pressure swing adsorption unit, V-104. Because the syngas produced in this plant has the main purpose of feeding a low temperature Fischer-Tropsch plant using a cobalt catalyst, the H_2/CO ratio needs to be lowered from 4.78 to 2. By specifying a 80 % recovery of H_2 (typical value) (Song, 2009) in V-104, it is possible to obtain a stream with 99.6 % H_2 which can be divided in two different streams: 27 % is added to stream 36 to adjust the H_2/CO ratio to 2 (because more H_2 is removed than needed) and the remaining can be sold for further treatment to be used in fuel cells. This approach of separating and then adjusting the ratio allows for more flexibility of the feed ratios for the Fischer-Tropsch process. Table 4-4 presents temperature, pressure and mass flow rate data of the process inlets and outlets.

Table 4-4. Process inlets and outlets data.

	Inlets		Outlets		
Stream	PREPGN	FEEDW	H2	CO2	SYNGASFT
T **(°C)**	20.0	14.9	50.0	50.0	49.5
P **(bar)**	13.8	1.00	31.9	32.4	31.9
W **(tonne·h^{-1})**	5.72	6.01	0.979	4.24	6.51

4.1.5 Energy integration network

In order to re-use as much as possible the heat released during the process, a network of heat exchangers was created, as illustrated in Figure 4-2. During the process of building the process flowsheet in Aspen Plus®, every heat exchanger/utility were represented by a heater block. After global process mass balance was concluded, a supplementary software, called Aspen Energy Analyzer® V9, which is an energy management software for performing optimal heat exchanger network design to minimize process energy, was used to integrate the plant wasted

heat, by building a network of heat exchangers that exchange heat with the process streams to improve the energy integration and to decrease the process costs.

To start the energy analysis, it is necessary to gather values of some temperature dependent physical properties of the streams that can exchange heat at the industrial plant (the process streams able for integration were 2, 9, 13, 19, 20, 30, 32, 33, GN and STEAM), such as viscosity, density, thermal conductivity and enthalpy. With that data, it is possible to construct the Composite Curves from Figure 4-3 and the Grand Composite Curve from Figure 4-4, two of the tools used in the Pinch methodology.

The Composite Curves consist of temperature-enthalpy profiles of heat availability (the hot composite curve) and heat demands (the cold composite curve) in the process. This graphical representation provides a counter-current picture of heat transfer and can be used to indicate the minimum energy target for the process. Its construction starts by considering zero enthalpy at the lowest temperature of the hot streams (36.9 °C) and the following values of the hot composite curve are obtained by adding the enthalpy changes of the streams in the respective temperature intervals.

The construction of the cold composite curve is similar to the hot one but involves the combination of the cold stream T-H curves for the process. The overlap of the two curves shows the maximum process heat recovery possible, indicating that the remaining heating and cooling needs are the minimum hot utility requirement (Q_{Hmin}) and the minimum cold utility requirement (Q_{Cmin}) of the SMR process for the chosen minimum temperature approach (ΔT_{min}) of 20 °C (typical value for hydrogen plants) (Linnhoff March, 1998).

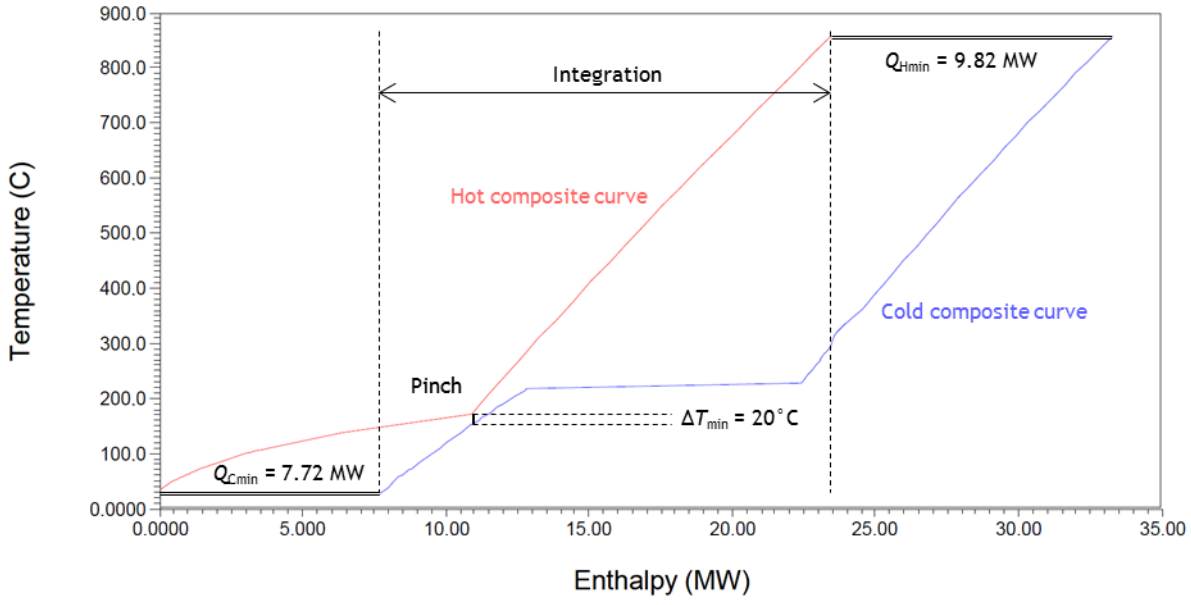

Figure 4-3. Composite curves of the SMR process.

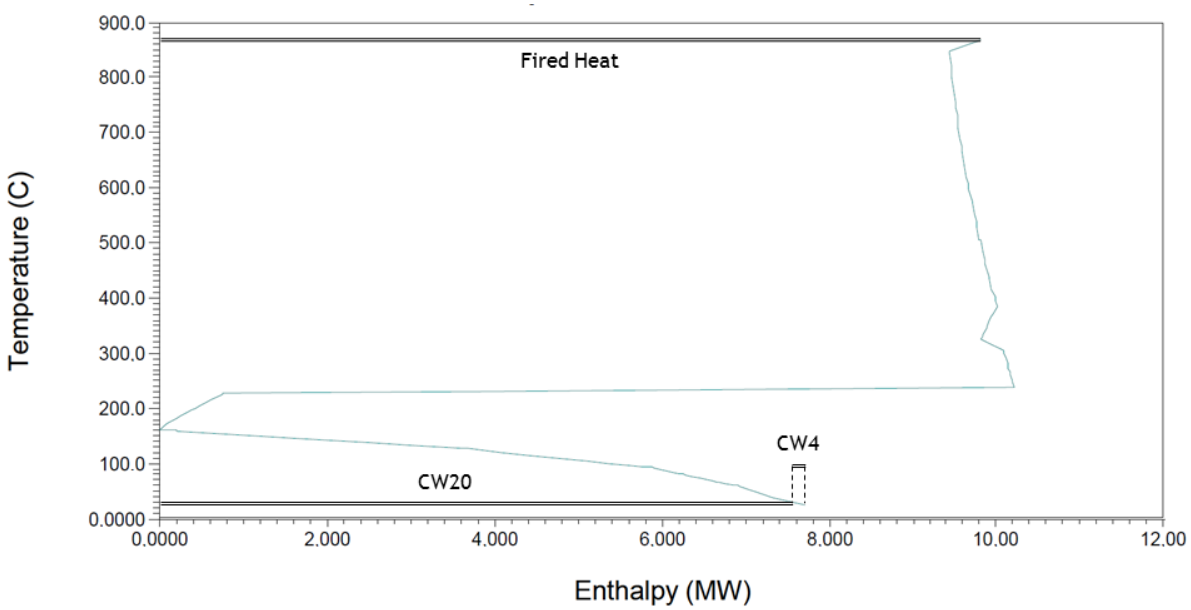

Figure 4-4. Grand Composite Curve for the SMR process.

The Grand Composite Curve is the other tool used in the Pinch analysis (Linnhoff March, 1998) and enables setting multiple utility targets easier. This curve is created from the composite curves by adjusting their temperatures (increasing the cold composite temperature by $^1/_2\,\Delta T_{min}$ and decreasing the hot composite temperature by $^1/_2\,\Delta T_{min}$ until the curves intersect each other at a point, named pinch point. The Grand Composite Curve is then obtained from the enthalpy differences between the new curves at different temperature. The point where enthalpy is zero marks the pinch (at 164 °C in this case) (Linnhoff March, 1998).

Analysing Figure 4-4, it is possible to identify 3 different utility types required by the process. Above pinch, where only hot utilities can be used, there is the need of a methane fuelled furnace operating between 400 °C and 1000 °C. In a typical SMR plant, this furnace would be the fired reformer itself, responsible for heating the reaction tubes and pre-heating the process streams through the heat of combustion gases. In the studied case, the furnace presented in Figure 4-2 is simulated using an RGibbs reactor (H-101), which estimates the combustion performance by minimizing the Gibbs free energy. The following combustion reaction (Equation 4.1) and inlet flows presented in Table 4-5 (stream 49 is air (21 wt.% O_2 and 79 wt.% N_2) and stream 50 only has methane for simplification purposes) are considered in order to obtain an outlet stream at 1000 °C to match Aspen Energy Analyzer® results and enough heat to keep the reactor H-101 running at a constant temperature.

$$CH_4 + 2O_2 \rightarrow 2H_2O + CO_2 \qquad (4.1)$$

Table 4-5. Furnace inlets and outlets data.

	Inlets		Outlets		
Stream	49	50	51	53	56
T **(°C)**	20.0	20.0	1 000	583	314
P **(bar)**	1.20	13.9	1.20	1.10	1.00
W **(tonne·h^{-1})**	40.5	2.13	42.6	6.18	36.4

Below pinch, two different cooling utilities were chosen: cooling water entering at 20 °C and exiting at 30 °C (suitable to be sent to a cooling tower and then to a watercourse), and cooling water entering at 4.44 °C and exiting at 10 °C. The latter is more expensive due to the refrigeration process associated and was only considered to satisfy the ΔT_{min}. For this reason, 98.8 %, of the waste heat is removed by a high flow of cooling water at 20 °C, resulting in lower consumption of cold water and operation costs.

After analysing all the curves, a possible heat exchanging network is created, capable of using the maximum process heat and minimizing the energy target for the process. The network can be consulted in Appendix E. The final integration network within the process itself is already represented in Figure 4-2.

4.2 Industrial plant cost estimation

To evaluate the economic potential of the process disclosed in the present work, a NETmix-based SMR industrial plant, two types of costs were estimated: CAPEX and OPEX.

The capital expenditure, CAPEX, are funds invested by a company to acquire, upgrade and maintain physical assets such as property, industrial buildings or equipment. If an expense is a capital expenditure, it needs to be capitalized, which requires the company to spread its fixed cost over the useful life of the asset. On the other hand, OPEX is an expense a business incurs through its normal business operations and can include inventory costs, marketing, payroll and R&D. Unlike capital expenditures, who undergo depreciation, revenue expenses can be fully tax-deducted in the same year they occur (Investopedia, 2018a, Investopedia, 2018b).

4.2.1 CAPEX

To start estimating capital expenditures based on the flowsheet created, the software Aspen Process Economic Analyzer V9, which is integrated with the process simulator used and relies on a model-based estimation to generate project capital cost estimates and investment

analysis, is used. This version presents equipment costs for the first quarter of 2015, and the chosen currency is US dollars.

The equipment sizing and direct cost estimation (including installation and manpower) is performed for pumps (P-101 to P-105), heat exchangers (E-101 to 103, E-105 and E-108 to E-111), vessels (V-101 to V-104), furnace (H-101), chiller and cooling tower (T-101). The missing heat exchangers were not designed since they only represent the heat exchange between the combustion gases from the furnace and the process streams circulating through coils inside the furnace, not being physically present. Moreover, reactor cost is calculated separately, since the software is not capable to determine the cost of a NETmix® device.

On a first step, simulation data from the Aspen Plus® is loaded to the cost estimator software. Next, the material for the centrifugal pumps are chosen using the pump sizing calculator from Grundfos product centre (Grundfos, 2018): SS304 for P-101, SS316 for P-102 and P-103 and cast iron for P-104 and P-105. Both compressors are built in carbon steel and have only one stage due to the relatively low compression ratios (below 3, 2 and 1.8 for C-101 and C-102, respectively). The material chosen to construct the box type furnace is 321S, a high alloy steel capable of withstanding high temperatures. Even though the furnace operates at a maximum temperature of 1000 °C and the materials available in Aspen Process Economic Analyzer database only stand temperatures up to 815 °C, it is considered that the metal wall itself would be protected by a refractory lining. The designed box type furnace has a capacity greater than required because, besides pre-heating the process streams, it also supplies the heat required by the reactor, 15.3 MW, since it was not considered the combustion reaction inside the LabNETmix reactor.

Next, all heat exchangers were design as TEMA type BEM shell-and-tube, which means, they all possess an integral cover, a one pass shell and a fixed tube sheet. Also, they have a triangular tube pitch of 25.4 mm, which leads to a closer packing and a smaller size. Because the several heat exchangers operate at different temperatures, they own different sizes and materials. Table 4-6 gives a brief description of the standard dimensions of each 1-2 shell-and-tube heat exchanger designed.

The refrigeration unit, a carbon steel chiller, has the minimum standard refrigeration capacity of 180 kW, although only needing 96 kW, revealing an unnecessary capital cost with larger than needed equipment because of the small scale of the industrial plant. The first packed tower, V-101, is designed using typical height and diameter values for packed columns, 13.7 m and 2.7 m (between 2.4 and 3 m) (Couper et al., 2010). The desulphurization column is made of A516 steel and the packing, due to the lack of a ZnO packing in the program database, is activated carbon. The V-102 is also made of A516 but it is designed as a vertical vessel with 1.2 m of diameter and 3.8 m of height. Finally, two PSA units, V-103 and V-104., are composed

by two activated carbon packed columns each, whose diameter and height, 3.9 m and 5 m, respectively, were obtained from the flow and dimensions of the columns used in the paper from Ribeiro et al., 2012.

Table 4-6. Material and dimensions of the designed heat exchangers.

Equipment	Tube material	Tube length (m)	Shell material	Nº shells/ diameter (m)
E-101	A214	4.9	A285C	1/0.9
E-102	A214	4.9	A285C	2/0.9
E-103	304W	4.9	SS304	2/0.9
E-105	304W	4.9	SS304	1/0.9
E-108	304W	2.4	SS304	1/0.6
E-109	A214	4.9	A285C	1/0.6
E-110	A214	4.9	A285C	3/0.9
E-111	A214	4.9	A285C	1/0.3

The cost of the LabNETmix reactor, R-101, is assessed from its weight and the price of steel. The type of stainless steel chosen to build the reactor was SS 304, which withstands a continuous service temperature up to 925°C (The Stainless Steel Information Center, 2018) and costs 3.75 US$·kg^{-1} (MetalMiner, 2018). First, a volume of steel of 13.5 m^3 was estimated for the LabNETmix module for SMR, composed by two steel covers, two combustion plates, two steel separators and a reaction plate, as illustrated in Figure 4-5.

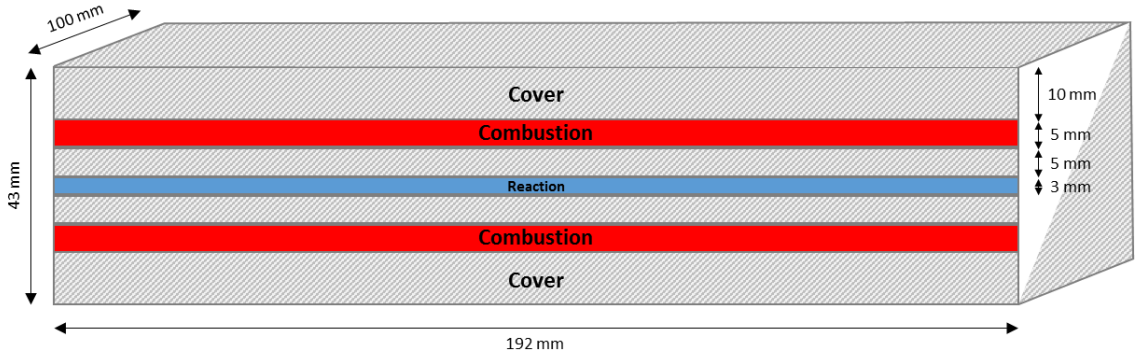

Figure 4-5. Scheme of a side cut of a LabNETmix module for SMR.

Considering that this module has to be repeated 70 455 times (to achieve the necessary reaction volume) the scaled-up LabNETmix reactor occupies approximately 22.0 m^3, which is substantially smaller than a typical industrial top fired methane steam reformer, which can reach volumes as high as 300 m^3 for a feed molar flow four times lower than the used one

(Zamaniyan et al., 2008). Also, the scaled-up reactor weights 108 metric tonnes and costs US$ 405 000. The total direct cost of R-101, assuming a cost multiplier of 1.6 for multi tubular stainless steel reactors (Couper et al., 2010), the final cost is US$ 648 000.

The equipment cost and the direct cost for each described equipment can be consulted in Appendix F.

Finally, with the total direct costs of the equipment, it is possible to determine CAPEX through Equation 4.2 (Cussler and Moggridge, 2011). It is assumed that the plant has an economic lifespan of 30 years and an interest rate of 10 %.

$$\text{CAPEX} = \frac{\sum_k C_{equip,k}}{N_{hours/year}\, \dot{P}_{syngas}} \frac{(1+rate)^{N_{years}}}{N_{years}} \tag{4.2}$$

where $C_{equip,k}$ is the direct cost of the equipment k, $rate$ is the interest rate, $\dot{P}_{syngas}$ is the productivity for syngas (H_2 and CO), expressed in metric tonnes per hour, $N_{hours/year}$ is the number of operating hours per year, which was assumed 8 760 hours (operating 24 hours per day, 7 days per week, 365 days per year), and N_{years} is the economical lifespan. At last, the CAPEX value for the simulated SMR industrial plant is US$ 156 per tonne of syngas.

4.2.2 OPEX

To calculate the OPEX costs for the simulated process, the main utilities considered were the methane feedstock for the furnace and electricity to power the cooling tower, the chiller, the pumps and the compressors. The utility prices considered are given in Table 4-7.

Table 4-7. Utility prices.

Utility	Price
Methane	0.19 US$·kg^{-1}
Electricity	57 US$·MWh^{-1}

With the methane feed flow to the furnace H-101 mentioned in Table 4-5, 2.13 tonne·h^{-1}, its lower calorific value, 15.4 kWh·kg^{-1}, its STP density, 0.80 kg·m^{-3}, (Engineering ToolBox, 2003) and its price (U.S. Energy Information Administration, 2018), it is possible to determine the normalized cost of keeping the furnace running, which totalizes US$ 72 per tonne of syngas.

Next, to calculate the cost of the electricity required for the cooling tower T-101, the demanded fan power was obtained (Peters et al., 2002). For a temperature range of 10 °C, the fans need 40.0 kW to cool down 0.18 m^3·s^{-1} water to 20 °C, representing a cost of US$ 0.41 per tonne of syngas. For the chiller, it is assumed a COP, coefficient of performance, of 6, which means that the 95.5 kW of cooling power represent 15.9 kW of consumed electricity, costing

US$ 0.16 per tonne of syngas. Finally, the cost of pumping and compressing is US$ 0.27 and US$ 9.60 per tonne of syngas, respectively.

The final OPEX costs for the simulated SMR industrial plant are 82 US$ per tonne of syngas. Thus, for each tonne of syngas produced during the economical lifespan of 30 year of the SMR plant, it is necessary to invest US$ 238 shared between CAPEX and OPEX costs. These costs can be lowered by increasing the plant capacity to meet the minimum standard dimensions for some of the equipment, such as chillers, and by integrating the SMR process with the Fischer-Tropsch process, allowing a more efficient heat integration and lower furnace feedstock costs, which comprises almost 90 % of the operating costs.

5 Conclusion

The main goal of this work is to assess the possibility of operating a Steam Methane Reforming process, using the NETmix® technology as a substitute for the typical large fired reformers and shift reactors, as well as the simulation of a working SMR industrial plant.

The first step was to find an available micro structured reactor and a catalyst for SMR to obtain the kinetic expressions of the reaction. The work from Tonkovich et al., 2007 was chosen, which describes a micro tubular reactor from Velocys© with a rhodium supported catalyst for SMR used for performance tests. The case was modelled in Aspen Plus®, the elected software to model the process, and the kinetic expressions of Tonkovich et al., 2007 were input to the model. The simulated results agreed well with experimental data from the literature, with absolute errors lower than 10 %. Internal mass transfer limitations in the catalyst from Velocys© were confirmed based on a Thiele modulus of 21.5, clearly in the diffusional regime region.

Afterwards, the rhodium supported catalyst was adapted (by removing the support) to obtain a 200 nm layer of rhodium capable of being applied by sputtering onto a LabNETmix reactor. Studies of mass diffusivity limitations were also performed for this adapted catalyst. It was concluded that the system was at an intermediate regime, presenting a Thiele modulus of 2.00, and that only 48.3 % of the layer was indeed used for the reaction, showing that the thin layer of rhodium has a better performance than the supported catalyst due to faster kinetics associated to the removal of the support.

The next step was to combine the rhodium layered catalyst with a scaled-up LabNETmix reactor to design an industrial SMR plant. The main goal of combining a highly active catalyst and a micro structured reactor is downsizing the equipment, namely the steam reformer. This result is very attractive for offshore applications, where SMR is used to explore stranded natural gas reserves or in combination with Fischer-Tropsch to produce liquid synfuel. The simulated plant for the syngas production to feed a Fischer-Tropsch industrial plant capable of producing 250 barrels per day of synfuel uses a scaled-up LabNETmix reactor with approximately 22.0 m^3, capable of operating at a steam/CH_4 ratio of 3, 860 °C and 19.1-20.1 bar, producing 5.57 tonne·h^{-1} of hydrogen and carbon monoxide with a H_2/CO ratio of 2 and with a methane conversion of 78 %. The normalized CAPEX and OPEX values per tonne of syngas associated to the simulated SMR industrial plant are US$ 156 and US$ 82, respectively. The latter can be lowered by integrating the SMR process with the Fischer-Tropsch process, allowing a more efficient heat integration.

As a final remark, the NETmix® reactor has been shown to be a possible solution to the existing mass transfer problems and for the downsizing of SMR plants for Gas-to-Liquids applications.

6 Assessment of the work done

6.1 Objectives Achieved

As proposed in the introduction chapter, an Aspen Plus® simulation of a working SMR industrial plant with a NETmix® reactor and the estimation of CAPEX and OPEX were accomplished with success. It was possible to create a flowsheet for an industrial-scale plant where the typical steam reformer and the shift reactor were substituted by a scaled-up LabNETmix reactor. Also, the installation created produces enough syngas to feed a Fischer-Tropsch industrial plant producing 250 barrels per day.

To achieve the final flowsheet, some initial steps were taken. First, a rhodium supported catalyst was retrieved from the literature and its associated kinetics were reproduced using Aspen Plus®, which allowed to validate the credibility of the paper used. Next, the catalyst and the kinetic expressions were adapted so it would resemble a catalyst applied by sputtering. A theoretical approach to this problem allowed to create an image of how the new rhodium catalyst would be applied to the LabNETmix and to verify the presence of mass diffusivity limitations.

Thus, all the tasks proposed were accomplished with success.

6.2 Limitations and Future Work

From the beginning, this work was limited in terms of catalyst data. Because this was the first approach to SMR in a NETmix® reactor, there weren't previous studies for the catalyst or the process. Because of that, a catalyst found in the literature was studied and adapted. Also, the process was created from an already existent process from SIAD S.p.A., which features a typical steam reformer and shift reactor for production of hydrogen. Thus, although the operating conditions were kept the most similar possible to the reference plant, they may not be realistic for an installation with a micro structured reactor and a more active catalyst, usually not used at an industrial scale.

Other sources of deviations are the approximations and adaptations done, especially the increase of the kinetics by a factor of 10 to represent the increase of activity when removing the support. To verify this, tests of application by sputtering and kinetic studies would have to be done to obtain the correct kinetic parameters. Also, besides calculating the Thiele modulus, assuming only the diffusion of methane in the layer of rhodium, to verify the existence of mass diffusivity problems, experiments could also be done to verify the results. One way to detect

mass transfer limitations is to change the feed velocity, because, at a fixed residence time, higher flow velocity leads to higher mass transfer rate. If the reaction rate doesn't change with the change of flow rate, the mass transfer limitations are negligible. (Zhang et al., 2009)

The next step after simulating the SMR process using the LabNETmix reactor would be connecting this process to the Fischer-Tropsch process and assess the combined CAPEX and OPEX after streams and heat integration. Because the two combined processes are more efficient than separated, CAPEX and OPEX values would be more affordable, making the GTL process more attractive. Also, another possible future task would be the study of combustion of methane or natural gas on a NETmix® reactor as a way of providing heat for the SMR reaction.

6.3 Final Assessment

This dissertation was very challenging and rewarding. It allowed me to put in practice the simulation knowledge I obtained during my graduation and got me out of my comfort zone by making me think in a different way that I was used to.

Unfortunately, because there wasn't a concrete catalyst to study, retrieving one from the literature lead to approximations, which may have influenced the results.

I'm grateful I had the opportunity to start developing the Steam Methane Reforming process for a possible NETmix® application. Although the SMR process has been studied for many years, its application to micro structured reactors is somewhat recent and represents a new step in the industry: the downsizing of equipment.

7 References

- AASBERG-PETERSEN, K., CHRISTENSEN, T. S., DYBKJAER, I., SEHESTED, J., OSTBERG, M., COERTZEN, R. M., KEYSER, M. J. & STEYNBERG, A. P. 2004. Synthesis gas production for FT synthesis *In:* STEYNBERG, A. & DRY, M. (eds.) *Studies in Surface Science and Catalysis*. Elsevier.
- AASBERG-PETERSEN, K., NIELSEN, C. S. & JØRGENSEN, S. L. 1998. Membrane reforming for hydrogen. *Catalysis Today,* 46**,** 193-201.
- AMJAD, U.-E.-S., GONÇALVES LENZI, G., CAMARGO FERNANDES-MACHADO, N. R. & SPECCHIA, S. 2015. MgO and Nb_2O_5 oxides used as supports for Ru-based catalysts for the methane steam reforming reaction. *Catalysis Today,* 257**,** 122-130.
- ASPEN TECHNOLOGY. 2001. *Aspen Physical Property System* [Online]. Available: http://web.ist.utl.pt/ist11061/de/ASPEN/Physical_Property_Methods_and_Models.pdf [Accessed 11 June 2018]
- BALTRUSAITIS, J. & LUYBEN, W. L. 2015. Methane Conversion to Syngas for Gas-to-Liquids (GTL): Is Sustainable CO_2 Reuse via Dry Methane Reforming (DMR) Cost Competitive with SMR and ATR Processes? *ACS Sustainable Chemistry & Engineering,* 3**,** 2100-2111.
- CARBERRY, J. J. 1962. Mass diffusion and isothermal catalytic selectivity. *Chemical Engineering Science,* 17**,** 675-681.
- CARLSSON, M. 2015. Carbon Formation in Steam Reforming and Effect of Potassium Promotion. *Johnson Matthey Technology Review*, 59, 313-318.
- CARRARA, A., PERDICHIZZI, A. & BARIGOZZI, G. 2010. Simulation of an hydrogen production steam reforming industrial plant for energetic performance prediction. *International Journal of Hydrogen Energy,* 35**,** 3499-3508.
- CHUNG, C. K., LIAO, M. W., KHOR, O. K. & CHANG, H. C. 2013. Enhancement of pore size distribution in one-step hybrid pulse anodization of aluminum thin films sputtered on Si substrates. *Thin Solid Films,* 544**,** 374-379.
- COMPACTGTL. 2018. *Technology Overview* [Online]. Available: http://www.compactgtl.com/technology/overview/ [Accessed 21 June 2018].
- COSTA, M. F., FONTE, C. M., DIAS, M. M. & LOPES, J. C. B. 2017. Heat transfer performance of NETmix—A novel micro-meso structured mixer and reactor. *AIChE Journal,* 63**,** 2496-2508.

- COUPER, J. R., PENNEY, W. R., FAIR, J. R. & WALAS, S. M. 2010. *Chemical Process Equipment - Selection and Design (Revised 2nd Edition),* Burlington, Butterworth-Heinemann, 535, 726.
- CUSSLER, E. L. 2009. *Diffusion: Mass Transfer in Fluid Systems,* Cambridge, Cambridge University Press, 119-122.
- CUSSLER, E. L. & MOGGRIDGE, G. D. 2011. *Chemical Product Design,* Cambridge, Cambridge University Press.
- ENGINEERING TOOLBOX. 2003. *Fuels - Higher and Lower Calorific Values*. [Online]. Available: https://www.engineeringtoolbox.com/fuels-higher-calorific-values-d_169.html [Accessed 11 June 2018].
- EUROPEAN COMMISSION 2007. Reference Document on Best Available Techniques for the Manufacture of Large Volume Inorganic Chemicals - Ammonia, Acids and Fertilisers, 39-43.
- FONTE, C. M. 2013. *The NETmix Reactor: Application to High Added-Value Products*. PhD, Universidade do Porto.
- GOMES, P. J. 2011. *The NETmix® Reactor - Strategies for Optimizing Mixing and Development of New Reactor Designs*. PhD, Universidade do Porto.
- GOODFELLOW. 2018. *Fecralloy - Iron/Chromium - Foam* [Online]. Available: http://www.goodfellow.com/catalogue/GFCat4I.php?ewd_token=wjHSBS3dHQhoGdqW0dhWvWLwhqKn8M&n=nFdgH31GHIHK73oeLQ4Ab9wBTgCIHg&ewd_urlNo=GFCat411&Catite=FE083810&CatSearNum=2 [Accessed 18 Feb. 2018].
- GRUNDFOS. 2018. *Pump sizing*. [Online]. Available: https://product-selection.grundfos.com/front-page.html?custid=GMA&qcid=375478161 [Accessed 7 June 2018].
- HUGHES, M. 2014. *What Is Sputtering? Magnetron Sputtering?* [Online]. Available: http://www.semicore.com/what-is-sputtering [Accessed 21 Feb. 2018].
- INVESTOPEDIA. 2018a. *Capital Expenditure (CAPEX)* [Online]. Available: https://www.investopedia.com/terms/c/capitalexpenditure.asp [Accessed 7 June 2018].
- INVESTOPEDIA. 2018b. *Operating Expense* [Online]. Available: https://www.investopedia.com/terms/o/operating_expense.asp [Accessed 7 June 2018].

- JOHNSON MATTHEY. 2018. *Pre-reforming for hydrogen* [Online]. Available: http://www.jmprotech.com/pre-reforming-catalysts-refineries-johnson-matthey [Accessed 27 June 2018].
- KHODAKOV, A. Y., CHU, W. & FONGARLAND, P. 2007. Advances in the development of novel cobalt Fischer-Tropsch catalysts for synthesis of long-chain hydrocarbons and clean fuels. *Chem Rev,* 107**,** 1692-744.
- KIM, T. W., PARK, J. C., LIM, T.-H., JUNG, H., CHUN, D. H., LEE, H. T., HONG, S. & YANG, J.-I. 2015. The kinetics of steam methane reforming over a Ni/γ-Al_2O_3 catalyst for the development of small stationary reformers. *International Journal of Hydrogen Energy,* 40**,** 4512-4518.
- LARANJEIRA, P. E. 2005. *NETmix Static Mixer - Modelling, CFD Simulation and Experimental Characterisation.* PhD, Universidade do Porto.
- LARANJEIRA, P. E., MARTINS, A. A., LOPES, J. C. B. & DIAS, M. M. 2009. NETmix®, a new type of static mixer: Modeling, simulation, macromixing, and micromixing characterization. *AIChE Journal,* 55**,** 2226-2243.
- LINDE ENGINEERING. 2018. *Hydrogen*. [Online] Available: https://www.linde-engineering.com/internet.global.lindeengineering.global/en/images/H2_1_1_e_12_150dpi_NB19_4258.pdf?v=11.0 [Accessed 7 June 2018]
- LINNHOFF MARCH. 1998. *Introduction to Pinch Technology*. [Online] Available: https://www.ou.edu/class/che-design/a-design/Introduction%20to%20Pinch%20Technology-LinhoffMarch.pdf [Accessed 12 June 2018].
- LOPES, J. C., LARANJEIRA, P. E., DIAS, M. M. & MARTINS, A. A. 2005. *Network mixer and related mixing process.*
- LUNA, E. C., BECERRA, A. M. & DIMITRIJEWITS, M. I. 1999. Methane steam reforming over rhodium promoted Ni/Al2O3 catalysts. *Reaction Kinetics and Catalysis Letters,* 67**,** 247-252.
- MAITLIS, P. M. & KLERK, A. D. 2013. *Greener Fischer-Tropsch Processes for Fuels and Feedstocks,* Weinheim, Wiley-VCH Verlag GmbH & Co, 19-33.
- MAROT, L., DE TEMMERMAN, G., OELHAFEN, P., COVAREL, G. & LITNOVSKY, A. 2007. Rhodium coated mirrors deposited by magnetron sputtering for fusion applications. *Rev Sci Instrum,* 78**,** 103507.

- MBODJI, M., COMMENGE, J. M., FALK, L., DI MARCO, D., ROSSIGNOL, F., PROST, L., VALENTIN, S., JOLY, R. & DEL-GALLO, P. 2012. Steam methane reforming reaction process intensification by using a millistructured reactor: Experimental setup and model validation for global kinetic reaction rate estimation. *Chemical Engineering Journal,* 207-208**,** 871-884.
- METALMINER. 2018. *Stainless Steel* [Online]. Available: https://agmetalminer.com/metal-prices/stainless-steel/ [Accessed 8 June 2018].
- NIKOO, M. K. & AMIN, N. A. S. 2011. Thermodynamic analysis of carbon dioxide reforming of methane in view of solid carbon formation. *Fuel Processing Technology,* 92**,** 678-691.
- ORLINSKI, D., BARDAMID, A. F., KONOVALOV, V., KEDROV, V., KLASSEN, N., SHTAN, A., SHAPOVAL, A., SOLODOVCHENKO, S., STRUKOV, G., VOITSENYA, V., VUKOLOV, K. & YAKIMOV, K. 2000. Rhodium as the promising material for the first mirrors of laser and spectroscopy methods of plasma diagnostics in a fusion reactor. *Problems of Atomic Science and Technology,* 3**,** 67-69.
- PETERS, M. S., TIMMERHAUS, K. D. & WEST, R. E. 2002. *Plant Design and Economics for Chemical Engineers,* New York, McGraw-Hill.
- RIBEIRO, A. M., SANTOS, J. C., RODRIGUES, A. E. & RIFFLART, S. 2012. Syngas Stoichiometric Adjustment for Methanol Production and Co-Capture of Carbon Dioxide by Pressure Swing Adsorption. *Separation Science and Technology,* 47**,** 850-866.
- RICKARD SPECIALTY METALS & ENGINEERING. 2013. *Inconel 625* [Online]. Available: http://www.rickardmetals.com/products/inconel-625/ [Accessed 28 June 2018].
- ROSTRUP-NIELSEN, J. R. 2008. Steam Reforming. *Handbook of Heterogeneous Catalysis*. Wiley-VCH Verlag GmbH & Co. KGaA.
- SENGODAN, S., LAN, R., HUMPHREYS, J., DU, D., XU, W., WANG, H. & TAO, S. 2018. Advances in reforming and partial oxidation of hydrocarbons for hydrogen production and fuel cell applications. *Renewable and Sustainable Energy Reviews,* 82**,** 761-780.
- SONG, C. 2009. Introduction to Hydrogen and Syngas Production and Purification Technologies. *In:* LIU, K., SONG, C. & SUBRAMANI, V. (eds.) *Hydrogen and Syngas Production and Purification Technologies*, New Jersey, John Wiley & Sons, Inc.
- THE NATIONAL INSTITUTE FOR OCCUPATIONAL SAFETY AND HEALTH. 2016. *Rhodium (metal fume and insoluble compounds, as Rh)* [Online]. Available: https://www.cdc.gov/niosh/npg/npgd0544.html [Accessed 28 June 2018].

- THE STAINLESS STEEL INFORMATION CENTER. 2018. *High temperature properties* [Online]. Available: http://www.ssina.com/composition/temperature.html [Accessed 8 June 2018].
- THYSSENKRUPP. 2018. *Steam reformer box* [Online]. Available: https://www.thyssenkrupp-industrial-solutions.com/en/products-and-services/fertilizer-plants/ammonia-plants-by-uhde/steam-reforming/steam-reformer-box/ [Accessed 21 June 2018].
- TONKOVICH, A., KUHLMANN, D., ROGERS, A., MCDANIEL, J., FITZGERALD, S., ARORA, R. & YUSCHAK, T. 2005. Microchannel Technology Scale-up to Commercial Capacity. *Chemical Engineering Research and Design*, 83, 634-639.
- TONKOVICH, A. Y., PERRY, S., WANG, Y., QIU, D., LAPLANTE, T. & ROGERS, W. A. 2004. Microchannel process technology for compact methane steam reforming. *Chemical Engineering Science*, 59, 4819-4824.
- TONKOVICH, A. L., ROBERTS, G., FITZGERALD, S. P., NEAGLE, P. W., QUI, D., SCHMIDT, M. B., PERRY, S. T., HESSE, D. J., LUZENSKI, R. J., CHADWELL, G. B., PENG, Y., MATTHIAS, J. A., GANO, N. P., LONG, R. Q., ROGERS, W. A., ARORA, R., SIMMONS, W. W., YANG, B. L., KUHLMANN, D. J., WANG, Y., YUSCHAK, T. D., FORTE, T., MONAHAN, J. A. & JETTER, R. 2015. *Integrated combustion reactor and methods of conducting simultaneous endothermic and exothermic reactions*. USA patent application US9192929B2.
- TONKOVICH, A. L. Y., YANG, B., PERRY, S. T., FITZGERALD, S. P. & WANG, Y. 2007. From seconds to milliseconds to microseconds through tailored microchannel reactor design of a steam methane reformer. *Catalysis Today*, 120, 21-29.
- U.S. ENERGY INFORMATION ADMINISTRATION. 2018. *Natural Gas Prices* [Online]. Available: https://www.eia.gov/dnav/ng/ng_pri_sum_dcu_nus_a.htm [Accessed 11 June 2018].
- VITA, A., CRISTIANO, G., ITALIANO, C., PINO, L. & SPECCHIA, S. 2015. Syngas production by methane oxy-steam reforming on Me/CeO_2 (Me=Rh, Pt, Ni) catalyst lined on cordierite monoliths. *Applied Catalysis B: Environmental*, 162, 551-563.
- WANG, Y., CHIN, Y. H., ROZMIAREK, R. T., JOHNSON, B. R., GAO, Y., WATSON, J., TONKOVICH, A. Y. L. & VANDER WIEL, D. P. 2004. Highly active and stable Rh/MgOAl2O3 catalysts for methane steam reforming. *Catalysis Today*, 98, 575-581.
- WANG, Y. C., YA-HUEI; GAO, YUFEI 2004. *Carbon nanotube-containing catalysts, methods of making, and reactions catalyzed over nanotube catalysts*. US6713519B2.

- ZAMANIYAN, A., EBRAHIMI, H. & MOHAMMADZADEH, J. S. S. 2008. A unified model for top fired methane steam reformers using three-dimensional zonal analysis. *Chemical Engineering and Processing: Process Intensification*, 47, 946-956.
- ZANFIR, M. 2014. Portable and small-scale stationary hydrogen production from micro-reactor systems. In: BASILE, A. & IULIANELLI, A. (eds.) *Advances in Hydrogen Production, Storage and Distribution*. Woodhead Publishing.
- ZDRAVKOV, B. D., ČERMÁK, J. J., ŠEFARA, M. & JANKŮ, J. 2007. Pore classification in the characterization of porous materials: A perspective. *Central European Journal of Chemistry*, 5, 385-395.
- ZHANG, J., WANG, H. & DALAI, A. K. 2009. Kinetic Studies of Carbon Dioxide Reforming of Methane over Ni−Co/Al−Mg−O Bimetallic Catalyst. *Industrial & Engineering Chemistry Research*, 48, 677-684.
- ZHAO, G., SUN, Q., WANG, X. & WANG, X. 2014. Natural Gas Transmission Pipeline Temperature Drop Calculation. *Advances in Petroleum Exploration and Development*, 7, 127-131.

Appendix A Water-Gas Shift reaction

The Water-Gas Shift reaction was discovered by the Italian physicist Felice Fontana in 1780 and it became industrially important when it was used to produce hydrogen for the Haber-Bosch ammonia synthesis.

In the reversible WGS reaction, carbon monoxide reacts with water over a catalyst to produce hydrogen and carbon dioxide. This reaction is used industrially together with SMR and DRM in hydrogen plants with the purpose of controlling (increasing, usually) the final H_2/CO ratio of the syngas produced. (Maitlis and Klerk, 2013).

$$CO + H_2O \rightleftharpoons CO_2 + H_2,\ \Delta H_{298} = -41\ kJ{\cdot}mol^{-1} \quad (2.2)$$

The WGS reaction is slightly exothermic and can be considered in equilibrium under most conditions. The temperature dependence of the equilibrium constant, K_2, is described by the following equation:

$$\log K_2 = \log\left(\frac{p_{CO_2} p_{H_2}}{p_{CO} p_{H_2O}}\right) = \left(\frac{2\,073}{T} - 2.029\right) \quad (A.1)$$

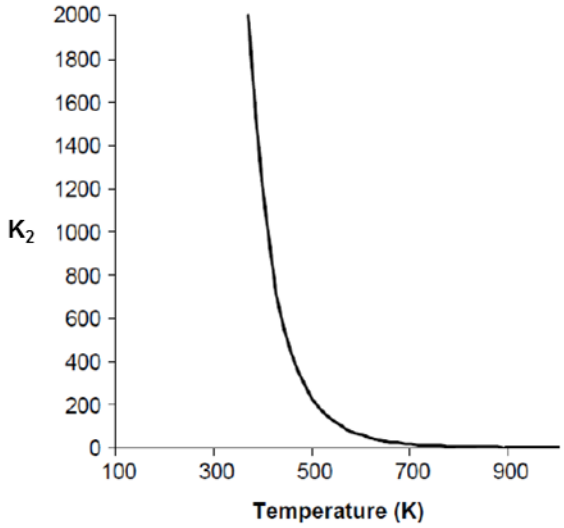

Figure A- 1. K_2 temperature dependence (Maitlis and Klerk, 2013).

The equilibrium constant dramatically lowers when the temperature increases from 200 to 600 °C, thus favouring a higher CO conversion at low temperatures. Industrially, the usual process includes two stages – HTS and LTS – in order to take advantage of the reaction kinetics and thermodynamics. In the first stage, a high temperature shift reactor operates around 320-500 °C with a Fe_2O_3-Cr_2O_3 catalyst, selected for its poisoning resistance and good selectivity. The reaction is quick due to the high temperature, although conversion is limited by the thermodynamic equilibrium. In the second stage, the reaction takes place in a low

temperature reactor at 200 °C and with a copper based catalyst. Due to the low activity of Fe-Cr catalysts below 350 °C, Cu-Zn oxides are the catalysts used, however, they are extremely susceptible to sulphur poisoning (Maitlis and Klerk, 2013).

Appendix B Rhodium-based catalyst preparation

The catalyst studied is a rhodium-based catalyst supported in MgO-Al_2O_3, developed by Velocys© in collaboration with the Pacific Northwest National Laboratory. As reported by Tonkovich et al., 2015, the catalyst is prepared by an incipient wetness method, where calcinated alumina powder is impregnated with an aqueous solution of magnesium nitrate hexahydrate, followed by another calcination period. The resulting material, an MgO-Al_2O_3 support, is further impregnated with an Rh nitrate solution, producing, after calcination, a catalyst powder containing 10 wt.% Rh, 6 wt.% MgO and 84 wt.% Al_2O_3.

After the zeolite is prepared, it is combined with deionized water to form a slurry, which is wash-coated onto a FeCrAlY felt (0.75 porosity) responsible for holding the catalyst inside the reactor. This metallic felt suffers a heat treatment to develop a thin layer of aluminium oxide, removing leak paths (Wang, 2004).

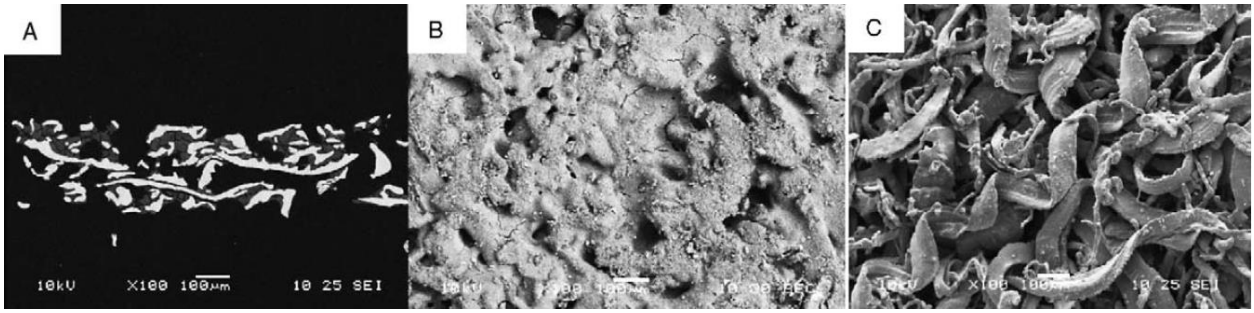

Figure B- 1. Cross-section (A) and surface (B) SEM micrograph of a wash-coated 10 wt.% Rh/MgO- Al_2O_3 over FeCrAlY felt engineered catalyst. SEM of uncoated FeCrAlY surface (C) is included for reference (Wang et al., 2004).

Appendix C Calculations and deductions

- Deduction of the mass balance equations for the catalyst layer present in Section 3.5.

The mass diffusivity limitations analysis was started by writing the mass balance over an infinitesimal volume element of catalyst, at steady-state:

$$Area\ \varphi_{\mathrm{z+dz}} = Area\ \varphi_{\mathrm{z}} + r\ Area\ \mathrm{d}z \tag{C.1}$$

$$\frac{\mathrm{d}\varphi}{\mathrm{d}z} = r \tag{C.2}$$

Where $Area$ is the cross section area of the catalyst layer, φ is the flux of methane, z is the position within the catalyst layer and r is the reaction rate in mol·cm^{-3}·s^{-1}. According to Fick's first law:

$$\varphi = \mathcal{D}_{eff}\frac{\mathrm{d}C_{CH_4}}{\mathrm{d}z} \tag{C.3}$$

And converting partial pressures of methane and water to concentrations, through ideal gas law:

$$r_1 = k_1 C_{\mathrm{CH_4}} C_{\mathrm{H_2O}} (RT)^2 \tag{C.4}$$

It's possible to obtain the following expression:

$$\mathcal{D}_{eff}\frac{\mathrm{d}^2 C_{\mathrm{CH_4}}}{\mathrm{d}z^2} - k_1 C_{\mathrm{CH_4}} C_{\mathrm{H_2O}} (RT)^2 = 0 \tag{C.5}$$

where $\mathcal{D}_{eff}$ is the effective diffusivity, k_1 is the pre-exponential factor of the rate equation, R is the universal gas constant and T is temperature. To make the solution independent of the problem scale, the latter equation was normalized in order of:

$$f_{\mathrm{CH_4}} = \frac{C_{\mathrm{CH_4}}}{C^s_{\mathrm{CH_4}}};\ f_{\mathrm{H_2O}} = \frac{C_{\mathrm{H_2O}}}{C^s_{\mathrm{H_2O}}};\ x = \frac{z}{l} \tag{C.6}$$

where $f_{\mathrm{CH_4}}$ and $f_{\mathrm{H_2O}}$ are the normalized methane and water concentrations, respectively, $C_{\mathrm{CH_4}}$ and $C_{\mathrm{H_2O}}$ are the methane and water concentrations, $C^s_{\mathrm{CH_4}}$ and $C^s_{\mathrm{H_2O}}$ are the methane and water concentrations at surface, respectively, x is the normalized position in the layer and l is the layer thickness.

After simplification, the Thiele modulus, Φ, and the normalized second order differential equation for the mass balance were obtained, assuming that $f_{\mathrm{H_2O}}$ is 1 because steam is fed to the system in excess.

$$\frac{\mathrm{d}^2 f_{\mathrm{CH_4}}}{\mathrm{d}x^2} - \Phi^2 f_{\mathrm{CH_4}} = 0 \tag{C.7}$$

$$\Phi = \sqrt{\frac{k_1 l^2 C^S_{\mathrm{H_2O}} (RT)^2}{\mathcal{D}_{eff}}} \tag{C.8}$$

To solve the mass balance, an RK23 algorithm, present in Appendix D, was run considering the following boundary conditions:

$$\begin{cases} x = 0; \ \frac{\mathrm{d}f_{\mathrm{CH_4}}}{\mathrm{d}x} = 0 \\ x = 1; \ f_{\mathrm{CH_4}} = 1 \end{cases}$$

- Deduction of the effectiveness factor expression

The effectiveness factor relates the average observed reaction rate, $\overline{r_{\mathrm{obs}}}$, with the reaction rate that would be observed if the whole catalyst was at surface conditions, $r_{\mathrm{t,s}}$.

$$\eta = \frac{\overline{r_{\mathrm{obs}}}}{r_{\mathrm{t,s}}} \tag{C.9}$$

From the Gauss' Theorem, which states that the consumption rate of methane is equal to its transfer rate by diffusion to the thin layer catalyst, $\overline{r_{\mathrm{obs}}}$ can be written as:

$$\frac{1}{V_{\mathrm{layer}}} \iiint r(V)\mathrm{d}V = A\mathcal{D}_{eff} \frac{\mathrm{d}C_{\mathrm{CH_4}}}{\mathrm{d}z}_{(z=l)} \tag{C.10}$$

Where V_{layer} is the volume for one layer. After normalization and simplification:

$$\eta = \frac{1}{\Phi^2} \frac{\mathrm{d}f_{\mathrm{CH_4}}}{\mathrm{d}x}_{(x=1)} = \frac{\tanh(\Phi)}{\Phi} \tag{C.11}$$

Appendix D Visual Basic code

The algorithm for the Runge-Kutta method implemented in Section 3.5 is divided in two sub functions:

- The first sub function is the algorithm itself;
- The second part is a sub function with the 1st order differential equation system to be solved;

The persons responsible for the writing of the visual basic code are mentioned on the beginning comments.

- **RK23 algorithm**

```
Sub RK_23()

'  Integracao de SEDOS por RUNGE-KUTTA
'  encaixados 2»-3» ordem
'  Escrito (em Basic) por M.R.N. Costa, FEUP, 1992
'  Traduzido para VBA por Madalena Dias, FEUP, 2015

   Dim E As Double, EPS As Double, H As Double
      Dim X() As Double, Y() As Double
   Dim F() As Double, F0() As Double
   Dim K1() As Double, K2() As Double
   Dim T As Double, T0 As Double, TF As Double
   Dim S As Integer, SMAX As Integer
   Dim I As Integer, J As Integer, N As Integer
   Dim t1 As Double

         Cells.Clear
          N = InputBox("numero de equacoes", , 2)
   ReDim Y(1 To N), X(1 To N), F(1 To N), F0(1 To N), K1(1 To N), K2(1 To N)

   T0 = InputBox("tempo inicial", , 0.00001)
   TF = InputBox("tempo final", , 1)
   EPS = InputBox("erro maximo", , 0.000000001)
```

```
For I = 1 To N
   Y(I) = InputBox("condicao inicial para Y(" & I & ")", , 0)
Next

Cells(1, 1) = "Passo"
Cells(1, 2) = "t"
For I = 1 To N
   Cells(1, I + 2) = "y(" & I & ")"
Next

H = (TF - T0) / (1 + 0.1 / Sqr(EPS))
SMAX = 10000
For S = 1 To SMAX
   Cells(S + 1, 1) = S
   Cells(S + 1, 2) = T0
   For I = 1 To N
      Cells(S + 1, 2 + I) = Y(I)
   Next
   If H * (T0 + H - TF) > 0 Then H = TF - T0

   T = T0
   For I = 1 To N
        X(I) = Y(I)
   Next
   Call funcao(N, T, F, X, t1)
   For I = 1 To N
      F0(I) = F(I)
   Next

   For J = 1 To 10
      For I = 1 To N
         K1(I) = H * F0(I)
         X(I) = Y(I) + K1(I)
      Next
      T = T0 + H
      Call funcao(N, T, F, X, t1)
      For I = 1 To N
         K2(I) = H * F(I)
```

```
            X(I) = Y(I) + 0.25 * (K1(I) + K2(I))
        Next
        T = T0 + 0.5 * H
        Call funcao(N, T, F, X, t1)
        E = 0
        For I = 1 To N
            F(I) = H * F(I)
            E = E + Abs(2 * F(I) - K1(I) - K2(I))
        Next
        E = E / (3 * N * EPS)
        If E < 1 Then Exit For
        H = H * 0.9 / Sqr(E)
    Next
    If J = 11 Then
        MsgBox "Passo diminuido 10x"
        Exit Sub
    End If

    For I = 1 To N
        Y(I) = Y(I) + (K1(I) + K2(I) + 4 * F(I)) / 6
    Next
    T0 = T0 + H
    If T0 >= TF Then
        Cells(S + 2) = S
        Cells(S + 2, 2) = T0
        For I = 1 To N
            Cells(S + 2, 2 + I) = Y(I)
        Next
        Exit Sub
    End If
    H = H * 0.9 / Sqr(E)
  Next
  MsgBox "Numero de passos excedido"

End Sub
```

- **Solving equation system from Section 3.5:**

  Variable change:

$$\begin{cases} \frac{df_{CH_4}}{dx} = p \\ \frac{dp}{dx} = \Phi^2 f_{CH_4} \end{cases}, \qquad \begin{cases} x = 0,\ f_{CH_4} = 1 \\ x = 1,\ \frac{df_{CH_4}}{dx} = 0 \end{cases}$$

```
Sub funcao(N, T, F, X, t1)
'
'   Atencao: se ocorrer uma divisao por T, nao comecar em T=0!
'            comecar por exemplo em T=1e-6

    t1 = (insert Thiele modulus)
    F(1) = X(2)
    F(2) = t1 ^ 2 * X(1)

End Sub
```

Appendix E Energy integration network

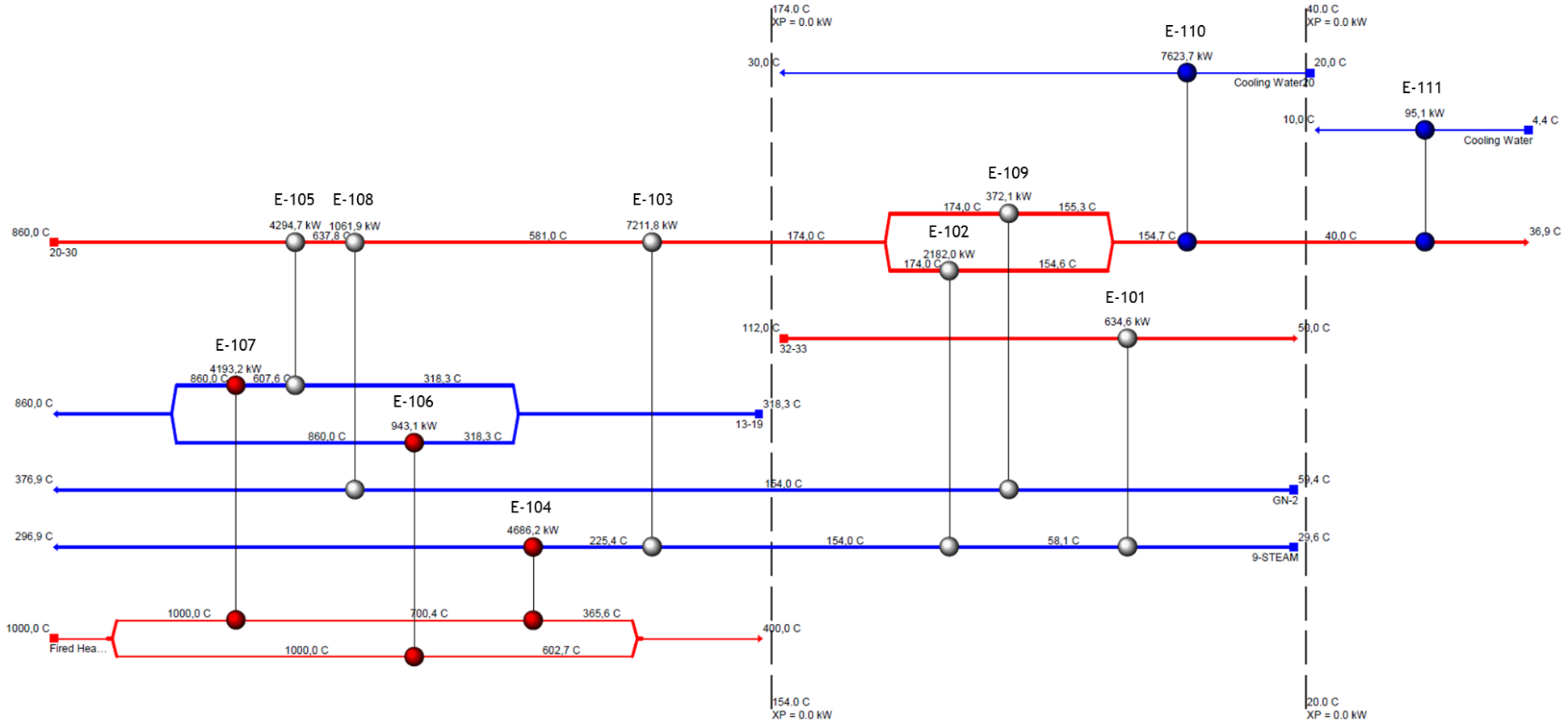

Figure E- 1. Heat exchanger network created with Aspen Energy Analyzer®.

Appendix F Equipment costs

		Thousand US$	
Equipment	**Type**	**Purchase cost**	**Direct cost**
P-101	Centrifugal single pump	45.4	5.2
P-102	Centrifugal single pump	60.4	22.8
P-103	Centrifugal single pump	59.2	6.5
P-104	Centrifugal single pump	107.9	16.3
P-105	Centrifugal single pump	35.9	4.1
C-101	Centrifugal horizontal compressor	882.6	745.7
C-102	Centrifugal horizontal compressor	1 400.6	1 246.4
H-101	Box type furnace	3 276.9	2 772.4
T-101	Cooling tower	350.5	198.6
E-101	BEM shell and tube heat exchanger	163.6	72.2
E-102	BEM shell and tube heat exchanger	284.6	151.3
E-103	BEM shell and tube heat exchanger	759.7	398.9
E-105	BEM shell and tube heat exchanger	1871	791
E-108	BEM shell and tube heat exchanger	220.1	95.7
E-109	BEM shell and tube heat exchanger	114.8	34.9
E-110	BEM shell and tube heat exchanger	361.1	214.4
E-111	BEM shell and tube heat exchanger	75.7	14.3
CHILLER	Refrigeration unit	180.1	114.9
V-101	Packed tower	683.1	229.4
V-103	Vertical vessel	105.7	23.9
V-104	Packed tower	681.4	357.2
V-102	Packed tower	681.4	357.2
R-101	LabNETmix	648.0	405.0
	Total	**US$ 13.0M**	**US$ 8.28M**